A cosmogenic ^{10}Be moraine chronology of arid, alpine Late Pleistocene glaciation in the Pioneer Mountains of Montana, USA.

Spruce W. Schoenemann[1], Mana M. Bryant[1], Will B. Larson[1], Lee B. Corbett[2], Paul R. Bierman[2]

Affiliations:
[1]Environmental Sciences Department, University of Montana Western, Dillon, MT 59725 USA
[2]Rubenstein School of the Environment and Natural Resources, University of Vermont, Burlington, VT 05405, USA

Corresponding author:
S Schoenemann, Email: spruce.schoenemann@umwestern.edu
Environmental Sciences Department, University of Montana Western, 710 S. Atlantic St. Dillon, MT, 59725 USA.

Keywords: surface exposure dating; mountain glaciation; moraines; paleoclimate reconstruction; terrestrial cosmogenic nuclides; Western United States; Late Pleistocene; Laurentide Ice Sheet

Abstract

We test the hypothesis that glacier systems, located in continental regions proximal to the Laurentide Ice Sheet (LIS), had local ice maxima considerably earlier than the LIS maximum and thus before the insolation minima at ~21 ka. Ranges located in the northwest US exhibit earlier deglaciation timing between ~23–22 ka, except for the Yellowstone region where younger time-transgressive ages complicate regional interpretations and the northern Montana ice cap where late glacial ages have recently been produced (Fig. 1). Constraining the glacial history of more ice sheet-proximal alpine glaciers provides insight into whether the contrasting maximum-ice times in the northern Rocky Mountains were caused by regional climatic differences, such as anticyclonic wind patterns driven by the presence of the LIS.

In the Pioneer Mountains of Montana, we measured *in situ* cosmogenic ^{10}Be in 35 boulders on moraines marking the maximum Late Pleistocene positions of alpine glaciers from three valleys. The ^{10}Be samples produced a range of ages, spanning pre Bull Lake to the last glaciation (i.e., Pinedale/Marine Isotope Stage (MIS) 2). We find an average exposure age for initial deglaciation of 18.2 ± 0.9 during the local Last Glacial Maximum, indicative of synchronous retreat in the Pioneer Mountains.

The similarity of initial deglaciation timing of the Pioneer Mountain glaciers with the northwestern Yellowstone glacial system and northern MT ice cap suggests that topography

more proximal to the LIS margin maintained full ice extent longer. Our findings, in context of previous work, suggest that in the case of the Pioneer Mountains their more proximal location to the ice margin may have delayed onset of deglaciation by greater exposure to local cooling from katabatic winds and/or additional moisture sourced from large ice-marginal glacial lakes, hence the lack of earlier deglacial ages like those found further to the west and east of the northern Rocky Mountain cordillera.

1. Introduction

Located south of the Cordilleran and Laurentide Ice Sheets (LIS), alpine glaciers occupied numerous mountain ranges across the western Cordillera during the latest Pleistocene, spanning a wide range of climatic zones that likely controlled glacier behavior (Laabs et al., 2020; Licciardi et al., 2004; Thackray, 2008). The pattern of glacial retreat during the last glaciation in the northwestern United States reveals regionally variable responses to shared climatic forcings (Laabs et al., 2020; Licciardi et al., 2004; Thackray, 2008), however, variability in the timing of deglaciation between regions appears to be related to climatic setting, differences in glacier mass balance characteristics (precipitation versus temperature), and changing atmospheric patterns driven by ice sheet growth and decay (Laabs et al., 2020; Licciardi et al., 2004; Licciardi and Pierce, 2018; Oster et al., 2015; Ullman et al., 2016, 2014; Wong et al., 2016).

Because glacier extent is controlled by both temperature and precipitation (Leclercq and Oerlemans, 2012; Oerlemans, 2005; Roe, 2011; Roe and O'Neal, 2009), it is often difficult to disentangle which of these parameters controlled glacier response to past climate fluctuations (Oerlemans, 2005). To evaluate which climatic factor might explain the significant timing differences among glacier maxima of the interior northwestern U.S., we focus on a once-glaciated range with an arid climate whose glacier response is thus likely to be temperature-dependent and controlled by solar insolation (Huybers and Roe, 2009; Roe and O'Neal, 2009; Rupper and Roe, 2008). We use cosmogenic ^{10}Be exposure dating of glacier moraines in the Pioneer Mountains of southwestern Montana to explore ice retreat timing and hence climate sensitivity in an arid region.

The Pioneer Mountains are well located to record responses of alpine glaciers to climate forcings (Fig. 1). Due to the proximity of the LIS margin (~250 km north of the Pioneer Mountains), the region's glacial climate would likely have been precipitation starved due to the dry, cold, katabatic winds descending off the ice sheet during the LGM (Oster et al., 2015). As deglaciation of the LIS commenced, the formation of pro-glacial meltwater lakes may have altered local precipitation patterns, supplying additional moisture relative to more distal alpine regions. Hence, these glaciated landforms archive valuable records of changes in temperature and regional precipitation, providing insight into the onset and drivers of deglaciation in the continental northwestern North America.

Previously published chronological data from the interior northwestern United States suggest that the glacial maxima observed in continental ranges (i.e., Wallowa, Wind River, and Big Horn mountains), followed insolation pacing, initiating deglaciation between 23–22 ka (Dahms et al., 2018; Laabs et al., 2020; Licciardi et al., 2004; Licciardi and Pierce, 2018; Phillips et al., 1997). Exposure ages from the northwestern (17.6 ka) and eastern (19.8 ka) greater Yellowstone glacial system (GYGS) do not show such an early response, and interpretation of its retreat timing is complicated by a migrating ice cap (Licciardi et al., 2001; Licciardi and Pierce, 2018, 2008). The goals of this study are to explore (1) differences in timing between alpine and LIS deglaciation timing, and (2) differences in timing between different mountain ranges in order to understand the impact of arid glacial environments and regional hydroclimate drivers.

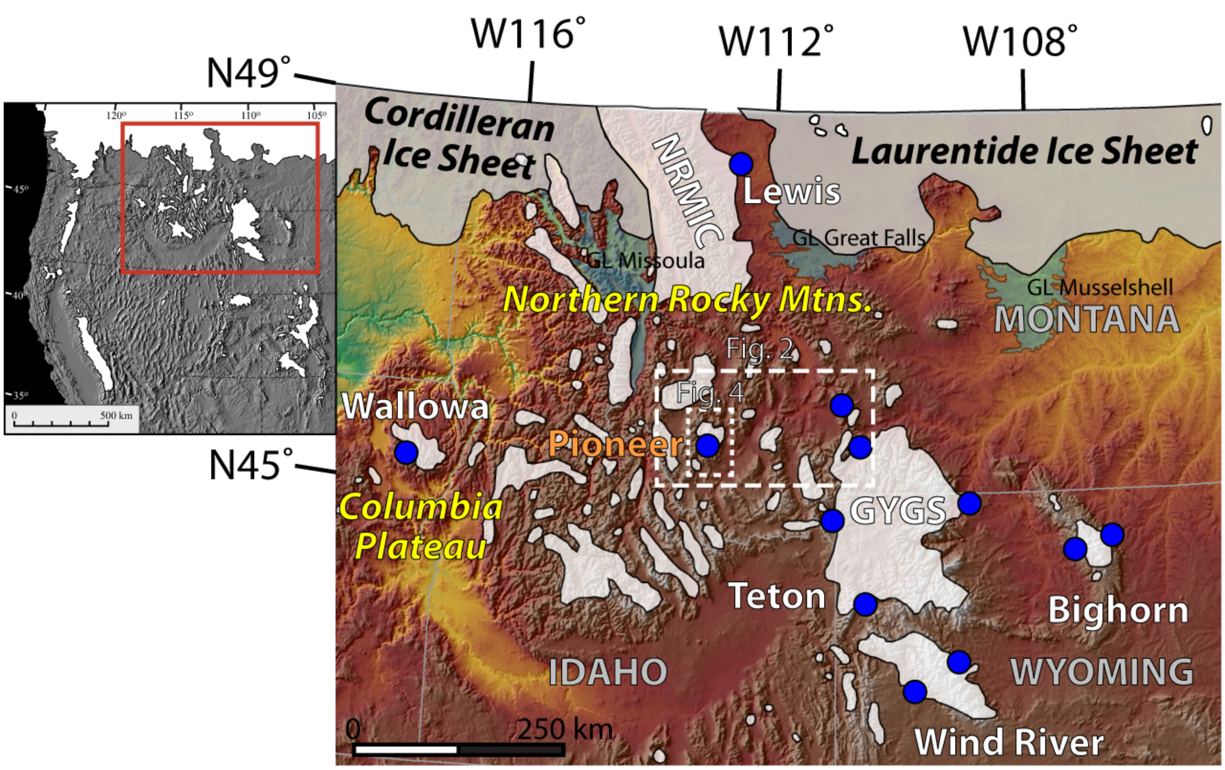

Figure 1. Map of Late Pleistocene mountain glaciation in the interior Northwest U.S and northern Rocky Mountains. Color relief map base produced from the National Map (http://www.usgs.gov/core-sciencesystems/national-geospatial-program/national-map). The Pioneer Mountains (orange label) are located at 45.5°N, 113°W. Physiographic regions described in the text are labeled in yellow. Mountain glacier systems are labeled in white, and redrawn from Porter et al. (1983) and Pierce (2003). Approximate locations of ice-sheet marginal glacial lakes (GL) outlined in blue. Circles indicate approximate locations of sites dated with exposure ages. NRMIC = Northern Rocky Mountain Ice Cap. Box indicates area shown in Fig. 2. Modified from Laabs et al. (2020) and Licciardi & Pierce (2018).

2. Previous work, study area, and study design

2.1 Previous work: Pioneer Mountains

In southwest Montana, glacial moraines, outwash, and erosional landforms indicate that many of the mountain ranges with land area above 2,500 m contained glaciers during the LGM (Locke, 1990; Porter, 1983). However, ice extent and glacier history are known only generally. Ice extents in the region are broadly delineated based on glacial geomorphic field mapping by Alden (1953). Glacial deposits mapped by Pearson and Zen (1985) and Ruppel et al. (1993) helped to further establish glacial extents, although slightly different limits were outlined by Locke and Smith (2004) who derived ice limits from map and aerial photo interpretation.

During Pleistocene glaciations, ice extent expanded in southwest Montana, producing small ice fields with outlet glaciers in some ranges and alpine glaciers that carved and filled mountain valleys, preferentially in north-northeast aspects. Evidence for previous glaciers include bowl-shaped cirques in the valley headwaters, which now contain small tarns or meadows, striations on bedrock, U-shaped valleys with obvious trimlines, erratic boulders, and moraines of bouldery till (Alden, 1953; Locke and Smith, 2004; Pearson and Zen, 1985). The east and west Pioneer Mountains are one of the largest ranges in the region (Fig. 2), and during the Pinedale glaciation (i.e. the last glaciation, as termed by Blackwelder, 1915 based on the type locale in Wyoming), ice on the ranges merged in the Wise River/Grasshopper drainages to form a small ice cap (Smith, 2007). According to Smith (2007), the east Pioneer ice cap may have been thick enough to form outlet glaciers that spilled across drainage divides near the headwaters of Wise River, Birch Creek, and Grasshopper Creeks (Smith, 2007, see Fig. 1).

Geomorphic descriptions of glacial landforms by Alden (1953) provide the earliest documentation of ice extent in western Montana. Alden explored many localities in the Beaverhead, Madison, Tobacco Root, and Pioneer Mountains between 1927 and 1938, and described both younger and older moraines and outwash plains that extended down valley of the glacial ice extent. In some valleys of the Pioneer Mountains, he identified older till with boulders containing large surface pits and moraines with subdued relief. Alden hypothesized that these landforms were formed during an earlier glaciation, and indeed, the differences in till characteristics are similar to those differences identified on confirmed Bull Lake and Pinedale moraines in the nearby West Yellowstone area by (Pierce, 2003). These early mapping efforts provided initial locations for Quaternary glacial deposits and have since been improved upon by Pearson and Zen (1985) and Locke and Smith (2004), although neither separated moraines from multiple glaciations. More recent regional surficial geology mapping efforts by McDonald et al. (2012) at 1:100,000 scale include the northeast portion of the Pioneer Mountains and McDonald and Yakovlev (2019) at 1:24,000 scale of Birch Creek valley provide more detailed glacial outlines. However, even these most recent maps of the Pioneer Mountains have not delineated between Bull Lake and Pinedale till deposits, nor glacial outwash, with some boundaries mistaking hillslope colluvium with till.

2.2 Study area: Pioneer Mountains, Montana

The Pioneer Mountains are located in southwestern Montana in a region characterized as arid-steppe-cold summer (BSk) based on the Köppen-Geiger climate classification (Peel et al., 2007). When the LIS was present, between ~35 and ~13 ka (Dyke, 2004; Fullerton et al., 2004; Stokes et al., 2012), the Pioneer Mountains were located within the anti-cyclonic katabatic winds that descended off the ice sheet (Oster et al., 2015; Wong et al., 2016). The isolated dome-shaped range is comprised of Cretaceous (~75 Ma) granodiorite of the Pioneer Batholith forming the north-south spine of the East Pioneer Mountains that rise to ~3200 m asl and Paleozoic metasedimentary rocks forming the more subdued peaks of the West Pioneers (Hyndman and Thomas, 2020).

The Pioneer Mountains are located east of the Continental Divide, in the orographic shadow of the Beaverhead Mountains which deplete moisture from the prevailing westerly winds. Today, the Pioneer Mountains receive the bulk of their precipitation in the winter and spring, with an average of 775 mm/year of water equivalent and a mean summer (JJA) temperature of 11˚C (1981-2021, Mule Creek station, 2530 m asl, NRCS). Major valleys along the eastern flanks of the Pioneer Mountains contained large valley glaciers (10–20 km length) during the Late Pleistocene. Although no ice remains, the semi-arid climate of southwest Montana has preserved many geomorphic features of the last glaciation (Smith, 2007).

2.3 Study Design

We selected multiple drainages in different sectors of the Pioneer Mountains with varying orientations to capture a range of physical and geomorphic characteristics that were most representative of the paleoglacier systems that once occupied the region. Of these, we narrowed down the selection to those glacial valleys that had well preserved glacial landforms, including lateral and terminal moraines. We attempted to find uneroded, undisturbed boulders for cosmogenic nuclide sampling. In some cases, we dated boulders on moraines that appeared to be the maximum lateral extent but were located considerably up-valley from the terminus; in other cases, we sampled some apparently older deposits based on their lack of obvious well-preserved terminus features from the prior glaciation (i.e., Bull Lake). In all, a total of 35 samples were collected from glacial deposits.

The three glacial valleys selected for sampling provide different orientations, hypsometry, lengths, shading, accumulation/ablation areas, and valley geometry (i.e., multiple cirque basins, pinch points, hanging valleys, etc.), representative of the variety of paleoglaciers that once filled the Pioneer Mountains (Fig. 2). Birch Creek valley was selected for its east aspect, which is the most common orientation for the larger valley glaciers, its moderate length, and prominent lateral moraine crests. Canyon Creek valley was selected for its unique northeast-facing aspect and greatest cirque-to-moraine length of the entire mountain range. Dingley Creek valley was selected for its west-facing aspect, short valley length, and simple geometry (i.e., single accumulation basin). Together, the three different glacial valleys offer a broad range of characteristics to explore how the timing of glacier retreat may differ within the range.

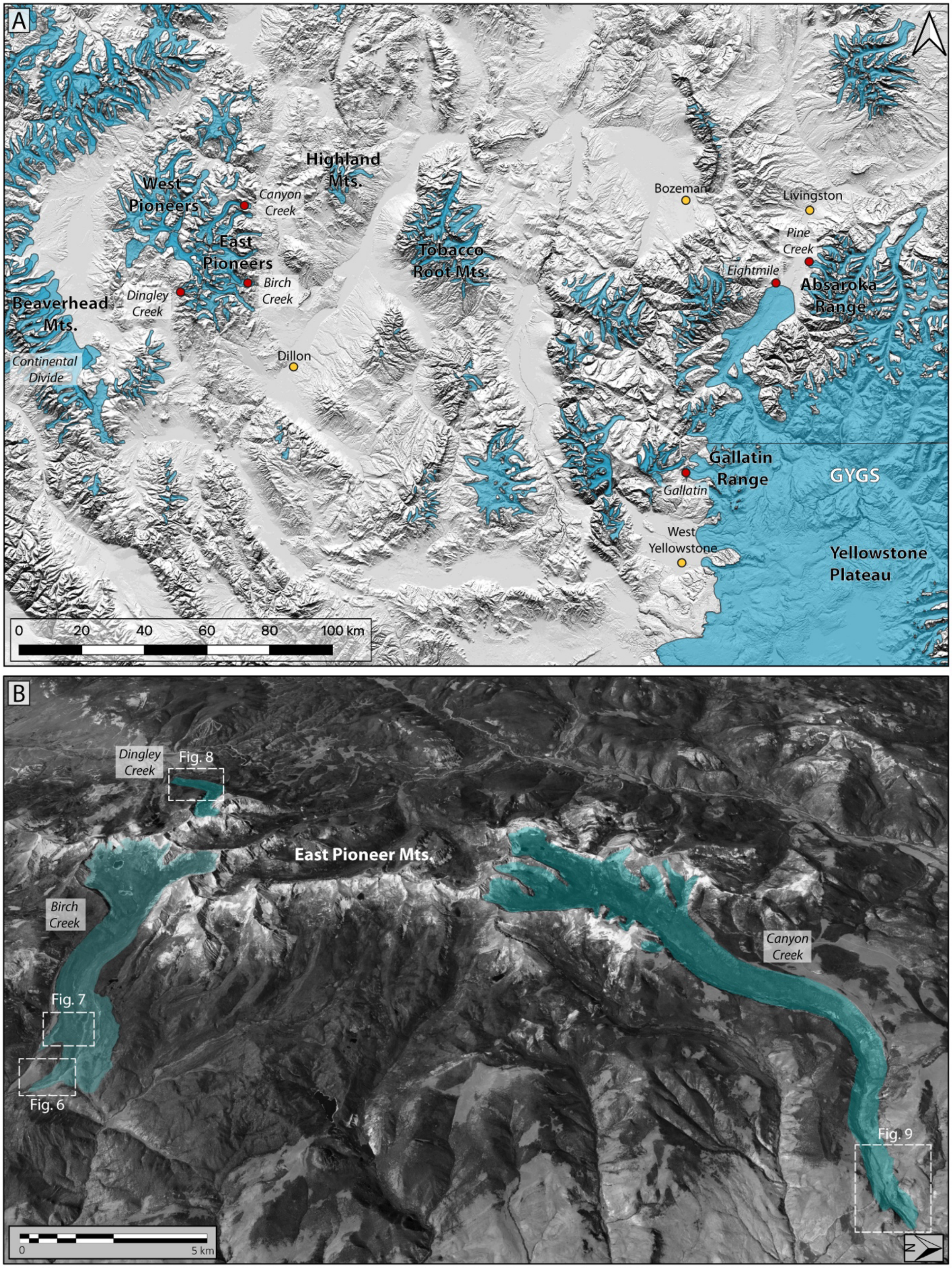

A
Highland
Mts.
West
Pioneers
Canyon
Creek
East
Pioneers
Birch
Creek
Dingley
Creek
Beaverhead
Mts.
Continental
Divide
Dillon
Tobacco
Root Mts.
Bozeman
Livingston
Pine
Creek
Eightmile
Absaroka
Range
Gallatin
Range
Gallatin
GYGS
West
Yellowstone
Yellowstone
Plateau
0
20
40
60
80
100 km
B
Dingley
Creek
Fig. 8
East Pioneer Mts.
Birch
Creek
Fig. 7
Fig. 6
Canyon
Creek
Fig. 9
0
5 km

Figure 2. A) Extent of Pinedale glaciation (outlines from Western US Paleoglaciers) of southwest Montana and northwest Greater Yellowstone Glacial System (GYGS) overlain on USGS shaded relief base map. Relevant mountain ranges (black), glacial valleys (italics) and sample locations (red circles) included. B) Oblique aerial view of the East Pioneer Mountains looking west (Google Earth). Erosional and depositional glacial landforms are visible along the north-south spine of the range. The blue outlines show the maximum glacial extent during the LGM of the three valleys sampled in this study. Canyon Creek, Birch Creek, and Dingley Creek study areas outlined in dashed white.

2.3.1 Birch Creek

Located on the eastern side of the Pioneer Mountains, the east-facing Birch Creek valley contains geomorphic evidence for a ~13 km-long valley glacier, ranging in elevation from ~3100 m to 1995 m (Fig. 2b). The upper valley is characterized by sharp aretes dissecting the accumulation area into three larger cirques with multiple tarns. The down-valley section of the glacier split into two lobes, with the second and more subtle left-hand lobe to the northeast having been identified by aerial imagery after field sampling (Fig. 2b). Much of the lower half of the glacier's extent is well outlined by lateral moraines, as well as some recessional moraines. The entire drainage sits within the Pioneer Batholith granodiorite.

2.3.2 Canyon Creek

The northeast-facing Canyon Creek valley contains glacial landforms extending ~23 km down valley (Fig. 2b), spanning elevations of ~3050 m to 1750 m. The head of the valley holds a cirque complex with three large cirques and multiple small cirques. The cirque basin is divided by numerous aretes, with threads of medial moraines leading downstream into a long u-shaped valley with mappable trimlines. Near the terminus a steep-sided roche moutonnee of quartzite crosses the valley floor obliquely, with a downstream medial moraine indicating that flow was split at one time, likely once the glacier receded from its maximum extent and thinned below the maximum height of the roche moutonnee (1907 m). The lithology of upper Canyon Creek consists of granodiorite and in the lower canyon, meta sedimentary sequences, including quartzite, dominate the valley.

2.3.3 Dingley Creek

Dingley Creek is located on the west side of the East Pioneer Mountains (Fig. 2b). The west facing valley has well-preserved glacial trimlines up-valley and lateral moraines down-valley, and it extends ~5 km from the cirque headwall to the terminus. The elevation ranges from ~2900 m to 2150 m. The upper valley is characterized by one cirque flanked by steep peaks to the east and south and a col to the north. The quartz-rich granodiorite dominated valley contains an abundance of large, semi-rounded boulders along the moraines. The glacier terminus is comprised of a steep end-moraine incised by the creek, with extensive hummocky ground till, a well-preserved, right-lateral moraine crest, and a more subtle, broad, left-lateral ridge.

3. Background: Cosmogenic nuclide dating techniques and applications

3.1 In-situ cosmogenic exposure dating: theory and assumptions

Terrestrial (in-situ) produced cosmogenic nuclides have been used since the 1990s to determine the timing and rates of deglaciation measured (Balco, 2011; Bierman, 1994; Fabel and Harbor, 1999; Phillips et al., 1990). The most commonly measured nuclide, ^{10}Be in quartz, accumulates at known rates in rock surfaces as they are exposed to high-energy cosmic radiation (Lal, 1988). The production rate of ^{10}Be is empirically constrained (Borchers et al., 2016); quantifying the abundance of the nuclide of interest in rock surfaces provides an integrated history about the exposure of that surface since deglaciation.

The interpretation of a cosmogenic nuclide measurement as an exposure age relies upon several key assumptions: (1) that the surface was deeply eroded during the most recent glaciation and nuclides from prior interglacial periods were removed (Briner et al., 2016), (2) that rock surfaces were not shielded by sediments or deep snow cover following deglaciation (Heyman et al., 2016; Schildgen et al., 2005), (3) that rock has not been removed from sampled surfaces by weathering or rock spalling after deglaciation (Zimmerman et al., 1994), and (4) that boulders (in the case of moraines) have not rolled or been exhumed from beneath eroding sediments. If these assumptions are not fully met, then calculated exposure ages under-estimate (in the case of post erosion, shielding, or boulder rolling) or over-estimate (in the case of prior inheritance of nuclides) the timing of actual surface exposure.

3.2 Applications of cosmogenic nuclide dating to Western US glacial history

Over the past three decades, the application of in-situ cosmogenic nuclide exposure dating to Late Pleistocene moraines in the western U.S. has produced hundreds of ages of alpine glacial features in the region (Dahms et al., 2010; Laabs et al., 2009; Licciardi et al., 2004, 2001; Licciardi and Pierce, 2018, 2008; Munroe et al., 2006; Phillips et al., 1997, 1990; Pierce, 2003; Thackray, 2008; Young et al., 2011). As reviewed in Laabs et al. 2020, cosmogenic nuclide exposure chronologies of moraines deposited during the last glaciation have been obtained for most major glaciated mountain ranges in the conterminous western United States including: the

Cascade Range and interior Pacific Northwest (e.g., (Licciardi et al., 2004; Porter and Swanson, 2008; Speth et al., 2018), the Rocky Mountains (e.g., (Brugger, 2007; Brugger et al., 2019b, 2019a; Gosse et al., 1995; Laabs et al., 2009; Leonard et al., 2017a; Licciardi et al., 2001; Licciardi and Pierce, 2008, 2018; Phillips et al., 1997; Young et al., 2011), the Colorado Plateau (e.g., (Marchetti et al., 2011, 2007, 2005), portions of the Basin and Range (e.g., (Laabs et al., 2013; Wesnousky et al., 2016), and the Sierra Nevada (e.g., (Nishiizumi et al., 1993; Phillips et al., 2009, 1996, 1990; Rood et al., 2011) (see Fig. 1).

Most of these studies have focused on determining the timing of glacial maxima by dating terminal moraines. When moraine crests were dated within a single mountain range or multiple moraine crests within a single glaciated valley, studies have found millennial-scale differences in the timing of maximum extent and/or timing of subsequent ice retreat (e.g., (Guido et al., 2007; Laabs et al., 2009; Leonard et al., 2017a, 2017b; Licciardi et al., 2004; Licciardi and Pierce, 2008; Marcott et al., 2019; Young et al., 2011). These chronologies have provided the basis for developing reconstructions of past temperature and precipitation and benchmarks for climate modeling during the last glaciation and deglacial transition in the western U.S. (Leonard et al., 2017a; Plummer and Phillips, 2003; Quirk et al., 2018; Refsnider et al., 2008)

Although a number of cosmogenic nuclide exposure chronologies exist from ranges in the Cascades (e.g., Icicle Creek near Leavenworth, WA, Porter and Swanson, 2008), the inland Pacific Northwest (e.g., Wallowa Lake near Joseph, OR, Licciardi et al., 2004), and greater Yellowstone (e.g., Beartooth Front near Livingston, MT, Licciardi and Pierce, 2008), there is a ~500 km gap spanning the northern Rocky Mountain region (Fig. 1). Besides a few radiocarbon ages derived from lake sediments in the Sawtooth Range, there are no exposure chronologies north of the Snake River Plain including central Idaho or southwestern Montana. Recent ages from the northern MT ice cap in Glacier National Park (e.g. Lewis Range) expand spatial coverage to the ice sheet margin (Quirk et al., 2022).

Studies using cosmogenic ^{10}Be exposure dating in the northwestern US have shown spatially variable Pinedale retreat timing between neighboring regions (Fig. 1; (Dahms et al., 2018; Laabs et al., 2020; Licciardi et al., 2004; Licciardi and Pierce, 2008; Phillips et al., 1997; Thackray et al., 2004). The LGM extents have been mapped and chronologies developed for a handful of ranges in the northwestern US including the Wallowa Mountains, OR, greater Yellowstone glacial system (GYGS: Beartooth Uplift, Absaroka Range, & Gallatin Range), Teton Range, WY, Bighorn Mountains, WY and Wind River Range, WY. The chronologies indicate bi-modal ages at some locations with an older and younger mode (i.e., Wallowa Mountains (22.8/18.5 ka), Wind River Range (22.1/18.7 ka) and Bighorn Mountain (22.9/18.0 ka), while chronologies from the Yellowstone glacial system indicate a time transgressive pattern moving from the northeast (i.e., Beartooth Uplift) to the southwest (Yellowstone Plateau). The existing LGM chronologies from the northern Rocky Mountains are based on ages from the GYGS which span a broad temporal range (e.g., 19.8 – 15.4 ka, Clarks Fork Canyon, WY to Jenny Lake, WY) driven by the migrating position of the Yellowstone ice cap (Licciardi and Pierce, 2018, 2008; Pierce, 2003; Pierce et al., 2018) and a limited number of ages from the Glacier National Park (e.g. Lewis Range, Quirk et al., 2022). The drivers of spatial heterogeneity of glacier responses in these northern ranges proximal to the LIS remains unclear.

4. Methods

4.1 Geomorphic and aerial mapping of landforms

In order to visualize large-scale glacial features remotely, we analyzed Landsat satellite imagery available through Google Earth Pro. Using the imagery, we identified terminal and lateral moraines with large boulders for potential sampling. In addition, we outlined polygons of the paleo-glacial extent based on trimlines and moraine crests to determine total area. Using a drone and photogrammetry software (Metashape by Agisoft), we created digital elevation models (DEMs) and orthophotos of glacial landforms for each glacier terminus in the study region. The high-resolution aerial imagery allowed us to identify subtleties in the glacial landforms and till extent. From the DEMs and imagery, along with ground truthing, we produced geomorphic maps of the termini that provided context for interpreting the cosmogenic exposure ages of the glacial boulders.

4.2 Sampling and field methods

To develop the first glacial chronologies for the Pioneer Mountains, we targeted the best preserved moraines mapped as Quaternary in age. For each valley, we selected boulders from well-preserved, outermost moraine crests. We collected samples during 2019 and 2020 from 35 boulder surfaces (Fig. 3, Table 1). We selected the largest boulders of granite and quartzite, standing at least >0.5 m above the ground to minimize potential complications related to cosmic-ray shielding by sediment and/or snow cover. We avoided boulders with obvious evidence of surface weathering (e.g., cm-scale weathering features), loss of mass (e.g., from fire or exhumation), or overturning. Most sampled boulders were large (~1–4 m), broad-based, and had rounded or flat upper surfaces with negligible surface pitting, with the exception of the quartzite boulders which tended to show some signs of frost shattering (Fig. 6f). We collected samples from boulder surfaces using a hammer and chisel.

At each sample site, we used handheld GPS (Garmin 64st, meter-scale accuracy) to record geographic coordinates and elevation; we measured boulder dimensions, the position of the boulder relative to the moraine crest, and topographic shielding using an inclinometer. In addition, we recorded the thickness of each sample, distance from boulder edge, and aspect of the boulder surface. Photographs were taken of the four cardinal locations and sampled area on the boulder. Sample elevations range from 1800 to 2350 m asl.

In the Birch Creek valley terminus, we collected six boulder samples (BC07–09, BC11–13) along the right lobe, from relatively broad moraine crests, but the terminus moraine itself had been mostly washed out with few in-place boulders (Fig. 4d). While the left lateral moraine had many optimal boulders (BC07–09), minimal boulders were present along the right lateral moraine (BC11–13) where the glacier deposited only a thin veneer of till that merged with colluvium derived from upslope. Although BC13 was located ~12 m below the moraine crest on a steep slope and was partly buried on the upslope side, it was the only large boulder positioned near the terminus (Fig. 4d, 6). Four additional boulders (BC01–04) were sampled along the outer crest of a prominent right lateral moraine ~4 km up valley from the terminus (Fig. 3a,d), with two boulders (BC05–06) sampled from a lower, nested, recessional moraine at the same location (Fig. 4d).

At Canyon Creek valley, we collected a total of twelve boulder samples. The complex terminus zone included a smaller right-hand lobe that was constrained by topography, a steep roche moutonnee in the center of the valley which produced a discontinuous medial moraine in its lee, and a high, subdued left-lateral moraine (see Fig. 4b). The lower right side of the terminus is not well defined by lateral or terminal moraines, so we collected four boulder samples ~800 m up valley within the right lobe (CC01–04). We gathered two samples (CC07, 09) along the crest of the medial moraine (Fig. 3c) and three sub-rounded granitic boulders (CC16, 17, 19) from the highest point on the roche moutonnee (Fig. 3e). The presence of large granitic boulders atop the quartzitic roche moutonnee indicate glacial ice overrode the landform during maximum ice thickness. Along the smoothed and weathered left-lateral moraine, only quartzite boulders were present, many of which were frost shattered and few above 0.5 m height (Fig. 3f). From these, we collected three samples (CC13–15).

In Dingley Creek valley, we sampled a total of eleven boulders (Fig. 4c). We collected four samples from the terminus (DC02–04, 11), three samples from the left lateral moraine (DC12–14) which onlapped the bedrock valley wall, and four samples (DC05, 06, 08, 10) from the well-defined right lateral moraine crest.

Table 1

Sample location information and field data for 35 boulder samples from the Pioneer Mountains, MT

Sample Name	Latitude (˚N)	Longitude (˚E)	Elevation (m a.s.l.)	Boulder Height (m)	Sample Thickness (cm)	Shielding corr.	Rock Type
Birch Creek Recessional							
BC-01	45.4230	-112.8877	2221	1.2	1.5	1.00	Granite
BC-02	45.4236	-112.8891	2266	1.8	10	1.00	Granite
BC-03	45.4238	-112.8913	2293	1.98	2	1.00	Granite
BC-04	45.4238	-112.8927	2319	0.61	6	1.00	Granite
BC-05	45.4252	-112.8869	2271	1.17	1.5	1.00	Granite
BC-06	45.4251	-112.8856	2267	1.8	4.5	1.00	Granite
Birch Creek Terminus							
BC-07	45.4252	-112.8556	2050	1.82	2	1.00	Granite
BC-08	45.4265	-112.8557	2075	1.98	3	1.00	Granite
BC-09	45.4276	-112.8564	2083	1.52	5	1.00	Granite
BC-11	45.4258	-112.8605	2057	0.57	3	1.00	Granite
BC-12	45.4264	-112.8628	2085	0.82	4	1.00	Granite
BC-13	45.4236	-112.8592	2042	0.75	8	0.99	Granite
Canyon Creek Terminus							
CC-01	45.6681	-112.7993	1908	0.76	3.5	1.00	Granite
CC-02	45.6686	-112.7942	1891	0.93	7	0.99	Granite
CC-03	45.6700	-112.7952	1872	1.98	5	0.97	Granite
CC-04	45.6697	-112.7951	1873	1.24	7	0.99	Granite
CC-07	45.6766	-112.7939	1806	0.5	2	1.00	Granite
CC-09	45.6747	-112.7964	1830	0.74	5.5	1.00	Quartzite
CC-13	45.6772	-112.7966	1808	0.59	4	1.00	Quartzite
CC-14	45.6772	-112.7970	1820	0.71	2	1.00	Quartzite
CC-15	45.6772	-112.7979	1831	1.45	8	1.00	Quartzite
CC-16	45.6730	-112.7997	1904	1.21	1.5	1.00	Granite
CC-17	45.6730	-112.7999	1900	1.32	3	1.00	Granite
CC-19	45.6735	-112.8013	1899	1.17	3	1.00	Granite
Dingley Creek Terminus							

DC-02	45.4305	-113.0832	2221	0.7	4	1.00	Granite
DC-03	45.4311	-113.0838	2229	0.74	3	1.00	Granite
DC-04	45.4318	-113.0842	2230	1.15	3	1.00	Granite
DC-05	45.4363	-113.0793	2354	0.57	5	1.00	Granite
DC-06	45.4362	-113.0799	2342	0.8	3	1.00	Granite
DC-08	45.4350	-113.0808	2311	1.26	4	1.00	Granite
DC-10	45.4345	-113.0825	2279	1.01	1.5	1.00	Granite
DC-11	45.4297	-113.0791	2241	2	5	0.99	Granite
DC-12	45.4299	-113.0771	2260	1.5	7	0.98	Granite
DC-13	45.4305	-113.0765	2285	1.5	5	0.97	Granite
DC-14	45.4313	-113.0755	2298	3	4	0.97	Granite

Figure 3. Photographs from the study area. A) View down-valley along right lateral moraine crest of Birch Creek (location of sample BC-03, 2293 m a.s.l.). B) Sub-rounded boulder on left lateral terminus of Birch Creek Valley (location of sample BC-07, 2050 m a.s.l.). C) Example of sub-angular quartzite boulder on medial moraine of Canyon Creek (location of sample CC-09, 1830 m a.s.l.). D) A typical granite boulder exhibiting subtle rounding (location of sample BC-01, 2221 m a.s.l.). E) Aerial view up-valley of rounded granitic boulders perched on the crest of a roche moutonnée exhibiting frost shattering of quartzitic bedrock in the Canyon Creek Valley (location of sample CC-19, 1899 m a.s.l.). F) Sampling boulder CC-15, which sits on the crest of the left lateral Bull Lake aged moraine in Canyon Creek (1831 m a.s.l.).

4.3 Sample preparation and isotopic analysis

We crushed and pulverized rock samples with a jaw crusher and disc pulverizer at Montana Technological University and isolated the 250 – 710 µm size fraction by sieving. We then isolated and purified quartz at the NSF/UVM Community Cosmogenic Facility following the methods of Kohl and Nishiizumi (1992) and verified quartz purity by Inductively Coupled Plasma Optical Emission Spectrometry.

We extracted beryllium (n = 35) in the NSF/UVM Community Cosmogenic Facility using methods described in Corbett et al. (2016) and ~20 g of quartz per sample. Samples were prepared in batches of 12, each of which included ten unknowns, one blank, and one quality control standard. We spiked each sample with ~250 µg Be using an in-house-made carrier, termed UVM-SPEX, created from a dilution of SPEX 1000 ppm Be standard, with a resulting Be concentration of 304 µg mL^{-1} (Table 2).

Accelerator Mass Spectrometry (AMS) analysis of $^{10}Be/^{9}Be$ occurred at the Purdue Rare Isotope Measurement (PRIME) Laboratory (Table 2). Sample analyses were normalized to primary standard 07KNSTD3110, with an assumed ratio of 2.850×10^{-12} (Nishiizumi et al., 2007). We corrected samples for backgrounds using the average and standard deviation of the four blanks associated with the samples ($4.6 \pm 1.1 \times 10^{-15}$) and propagated the blank uncertainties in quadrature. Background-corrected sample ratios range from 2.63 to 38.3×10^{-13}; analytic uncertainties (including the propagated blank uncertainty) are 2.1 ± 0.5 % (average, 1 SD).

Table 2

Sample preparation and laboratory information for $^{10}Be/^{9}Be$ analyses.

Sample Name	Quartz Mass (g)	Mass of ^{9}Be Added (μg)*	AMS Cathode Number	Uncorrected $^{10}Be/^{9}Be$ Ratio**	Uncorrected $^{10}Be/^{9}Be$ Ratio Uncertainty**	Background-Corrected $^{10}Be/^{9}Be$ Ratio	Background-Corrected $^{10}Be/^{9}Be$ Ratio Uncertainty	^{10}Be Concentration (atoms g^{-1})	^{10}Be Concentration Uncertainty (atoms g^{-1})
BC-01	22.056	250.1	163559	5.311E-13	1.266E-14	5.265E-13	1.271E-14	3.99E+05	9.63E+03
BC-02	21.972	253.0	163560	5.038E-13	1.220E-14	4.992E-13	1.225E-14	3.84E+05	9.42E+03
BC-03	21.724	250.8	163561	5.232E-13	1.263E-14	5.186E-13	1.268E-14	4.00E+05	9.78E+03
BC-04	21.926	251.8	163562	4.815E-13	1.561E-14	4.769E-13	1.565E-14	3.66E+05	1.20E+04
BC-05	22.107	250.6	163563	5.134E-13	1.286E-14	5.088E-13	1.291E-14	3.85E+05	9.78E+03
BC-06	21.901	250.3	163564	4.785E-13	1.200E-14	4.739E-13	1.205E-14	3.62E+05	9.20E+03
BC-07	21.459	251.0	163683	5.006E-13	1.343E-14	4.960E-13	1.347E-14	3.88E+05	1.05E+04
BC-08	21.350	249.8	163671	5.239E-13	1.437E-14	5.193E-13	1.441E-14	4.06E+05	1.13E+04
BC-09	21.382	250.6	163672	5.138E-13	9.660E-15	5.092E-13	9.723E-15	3.99E+05	7.62E+03
BC-11	17.843	250.4	163673	4.223E-13	7.802E-15	4.177E-13	7.880E-15	3.92E+05	7.39E+03
BC-12	21.476	251.0	163684	5.440E-13	1.225E-14	5.393E-13	1.230E-14	4.21E+05	9.61E+03
BC-13	20.983	250.0	163674	4.073E-13	7.737E-15	4.027E-13	7.816E-15	3.21E+05	6.22E+03
CC-01	21.438	249.8	163676	4.069E-13	1.078E-14	4.023E-13	1.083E-14	3.13E+05	8.44E+03
CC-02	21.463	249.5	163677	1.821E-12	3.392E-14	1.817E-12	3.394E-14	1.41E+06	2.64E+04
CC-03	12.891	250.4	163685	2.671E-13	6.449E-15	2.625E-13	6.543E-15	3.41E+05	8.49E+03
CC-04	21.488	249.8	163678	4.304E-13	7.973E-15	4.258E-13	8.050E-15	3.31E+05	6.25E+03
CC-07	15.404	250.7	163686	3.236E-13	7.360E-15	3.190E-13	7.443E-15	3.47E+05	8.10E+03
CC-09	21.585	249.7	163687	4.464E-13	9.730E-15	4.418E-13	9.793E-15	3.42E+05	7.57E+03
CC-13	16.004	250.0	163689	2.524E-12	2.531E-14	2.519E-12	2.533E-14	2.63E+06	2.64E+04
CC-14	16.673	249.8	163690	1.709E-12	1.927E-14	1.705E-12	1.930E-14	1.71E+06	1.93E+04
CC-15	15.407	250.5	163691	3.833E-12	3.450E-14	3.828E-12	3.452E-14	4.16E+06	3.75E+04
CC-16	21.508	250.7	163692	4.824E-13	1.047E-14	4.778E-13	1.053E-14	3.72E+05	8.20E+03
CC-17	21.657	250.0	163693	5.400E-13	9.079E-15	5.354E-13	9.146E-15	4.13E+05	7.06E+03
CC-19	21.555	250.7	163696	4.621E-13	9.357E-15	4.574E-13	9.422E-15	3.55E+05	7.32E+03
DC-02	21.288	250.8	163679	5.376E-13	8.822E-15	5.330E-13	8.891E-15	4.20E+05	7.00E+03
DC-03	21.536	250.2	163680	5.775E-13	9.313E-15	5.729E-13	9.379E-15	4.45E+05	7.28E+03
DC-04	15.879	249.3	163682	4.349E-13	9.482E-15	4.303E-13	9.547E-15	4.51E+05	1.00E+04

DC-05	21.522	249.1	163697	6.389E-13	1.025E-14	6.343E-13	1.031E-14	4.91E+05	7.97E+03
DC-06	21.581	249.4	163698	4.996E-13	8.761E-15	4.950E-13	8.831E-15	3.82E+05	6.82E+03
DC-08	21.522	249.1	163699	5.965E-13	1.018E-14	5.919E-13	1.024E-14	4.58E+05	7.92E+03
DC-10	21.525	250.3	163700	1.695E-12	2.027E-14	1.690E-12	2.030E-14	1.31E+06	1.58E+04
DC-11	14.378	251.3	163702	3.790E-13	7.500E-15	3.744E-13	7.581E-15	4.37E+05	8.85E+03
DC-12	21.505	250.3	163703	5.726E-13	9.364E-15	5.680E-13	9.429E-15	4.42E+05	7.33E+03
DC-13	21.524	250.9	163704	5.595E-13	1.739E-14	5.549E-13	1.742E-14	4.32E+05	1.36E+04
DC-14	21.542	249.1	163705	5.877E-13	1.113E-14	5.830E-13	1.119E-14	4.50E+05	8.64E+03

*^{9}Be was added through a carrier made at University of Vermont, termed UVM-SPEX, created from a dilution of SPEX 1000 ppm Be standard, with a resulting BE concentration of 304 µg mL^{-1}.

**Isotopic analysis was conducted at PRIME Laboratory; ratios were normalized against standard 07KNSTD3110 with an assumed ratio of 2.850 x 10^{-12} (Nishiizumi et al., 2007).

4.4 Exposure age calculations

We calculated cosmogenic ^{10}Be exposure ages using version 3.0 of the Online Exposure Age Calculator (OEAC, http://hess.ess.washington.edu/math/, last access: 27 February 2023) (Balco et al., 2008). The calculated ages assume no nuclides were inherited from previous exposure, no post-exposure erosion, no snow cover, a rock density of 2.65 g cm^{-3}, and the standard atmosphere model. In order to facilitate comparison with other glacial moraine exposure ages in western North America (e.g., Laabs et al., 2020), we calculated exposure ages using the time-dependent scaling method of Lifton et al. (2014) (LSDn) and the regional ^{10}Be production rates determined at Promontory Point, Utah (Balco et al., 2008; Lifton et al., 2015).

4.5 Age uncertainties

We report cosmogenic exposure ages of individual sample surfaces using both 1σ internal and external uncertainties (Table 3). We use the internal uncertainties when assessing relationships between samples in our dataset and the external uncertainties when comparing to other studies and other forms of chronology.

For each glacial valley, we calculated the timing of moraine occupation and abandonment as the arithmetic mean of all boulder exposure ages from the maximum extent of datable landforms. We first report these averages including all sample points, then explore whether a subset of the samples record processes other than simple deglaciation timing (e.g., surface burial, boulder rolling, fire spalling, recessional deposition, etc.). In the latter case, we then assess how the resulting averages would change based on the exclusion of possible outliers. To identify possible outliers, we use the OEAC's built-in landform outlier detection which calculates the p-value of the chi-squared statistic with respect to the mean, using measurement uncertainties, of the entire dataset by landform and/or valley (see Section 4C of the OEAC documentation).

The effects of snow cover on cosmogenic nuclide production are difficult to estimate, but were likely minimized by selecting relatively tall boulders (Schildgen et al., 2005). In most reports of exposure ages in the western U.S., the effects of snow cover on cosmogenic nuclide production have been assumed to be negligible (Laabs et al., 2020) and recent modeling studies by Ye et al., (2023) using modern and time-integrated snow cover suggest that in the Northern Rockies, wind-swept regions have minimal snow correction factors (e.g., Fig. 4, Ye et al., 2023). The modern-day down-valley moraine crests (~2100–2200 m) of the Pioneer Mountains generally receive minimal amounts of snow cover (SWE = 0.78 m/yr, Mule Creek SnoTel, 2530m, NRCS), and are often scoured by strong winds. As such, we assume that snow cover is negligible but note that snow cover would cause our reported ages to be minima.

4.6 Regional comparison of northern Rocky Mountain Last Glacial Maximum ages

The widespread application of exposure dating to moraines of the last glaciation throughout the Western US has provided numerous exposure ages that affords comparison of the timing of the Pinedale Glaciation in the Rocky Mountains. We compare our results of the last glaciation timing of the Pioneer Mountains with other northern Rocky Mountain moraines including the northwest portions of the greater Yellowstone glacial system (GYGS), Lewis Range, Teton Range, Big Horn Mountains, Wind River Range, and the Columbia Plateau (i.e., Wallowa Mountains), using comparable exposure ages recalculated by Laabs et al., (2020) with the LSDn scaling model and in-situ production rate from Promontory Point, UT (Lifton et al., 2015). To identify region-wide patterns in the timing of deglaciation, we grouped last glacial (MIS 2) exposure ages from each range that shared similar modes (i.e., old and young) and averaged them together for each mode to obtain a larger sample size (see Table 4). In the case of the GYGS, we included last glacial ^{10}Be exposure ages from the northwestern sector (see Fig. 1 in Licciardi and Pierce, 2018 for details): Eightmile (17.9 ± 1.2 ka), Pine Creek (18.2 ± 1.3 ka), South Fork Deep Creek (17.5 ± 1.1 ka), Cascade Canyon (16.9 ± 0.2 ka) and Gallatin River Valley (17.7 ± 0.4 ka), yielding an average age of 17.8 ± 1.1 ka (n = 24, 1 SD).

Table 3

Calculated exposure ages based on in situ ^{10}Be (n = 35) concentrations

Sample Name	Latitude (˚N)	Longitude (˚E)	Elevation (m a.s.l.)	^{10}Be Exposure Age (ka)[a]	^{10}Be Internal Uncertainty (ka)[a]	^{10}Be External Uncertainty (ka)[a]
Birch Creek Recessional (4 km up-valley)						
BC-01	*45.4230*	*-112.8877*	*2221*	*16.0*	*0.4*	*0.7*
BC-02	*45.4236*	*-112.8891*	*2266*	*16.0*	*0.4*	*0.7*
BC-03	*45.4238*	*-112.8913*	*2293*	*15.3*	*0.4*	*0.7*
BC-04	*45.4238*	*-112.8927*	*2319*	*14.3*	*0.5*	*0.7*
BC-05	*45.4252*	*-112.8869*	*2271*	*15.0*	*0.4*	*0.7*
BC-06	*45.4251*	*-112.8856*	*2267*	*14.5*	*0.4*	*0.7*
		Recessional (n = 6) avg ± st dev		15.2	0.7	
Birch Creek Terminus						
BC-07	45.4252	-112.8556	2050	17.7	0.5	0.8
BC-08	45.4265	-112.8557	2075	18.3	0.5	0.9
BC-09	45.4276	-112.8564	2083	18.1	0.4	0.8

BC-11	45.4258	-112.8605	2057	17.9	0.3	0.8
BC-12	45.4264	-112.8628	2085	19.0	0.4	0.8
*BC-13	45.4236	-112.8592	2042	15.7	0.3	0.7
			(n = 6) avg ± st dev	17.8	1.1	
			LGM (no outliers, n = 5) avg ± st dev	**18.2**	**0.5**	
Canyon Creek Terminus						
*CC-01	45.6681	-112.7993	1908	16.1	0.4	0.8
CC-02	*45.6686*	*-112.7942*	*1891*	*68.2*	*1.3*	*2.9*
CC-03	45.6700	-112.7952	1872	18.7	0.5	0.9
CC-04	45.6697	-112.7951	1873	18.0	0.3	0.8
CC-07	45.6766	-112.7939	1806	18.9	0.4	0.8
CC-09	45.6747	-112.7964	1830	18.8	0.4	0.8
CC-16	45.6730	-112.7997	1904	18.7	0.4	0.8
*CC-17	45.6730	-112.7999	1900	20.9	0.4	0.9
CC-19	45.6735	-112.8013	1899	18.2	0.4	0.8
			(n = 8) avg ± st dev	18.5	1.3	
			LGM (no outliers, n = 6) avg ± st dev	**18.5**	**0.4**	
Canyon Creek pre-LGM Composite Moraine						
CC-13	45.6772	-112.7966	1808	142.5	1.5	5.8
CC-14	45.6772	-112.7970	1820	90.6	1.1	3.7
CC-15	45.6772	-112.7979	1831	222.5	2.1	9.1
Dingley Creek Terminus						
DC-02	45.4305	-113.0832	2221	17.2	0.3	0.7
DC-03	45.4311	-113.0838	2229	17.9	0.3	0.7
DC-04	45.4318	-113.0842	2230	18.1	0.4	0.8
DC-05	45.4363	-113.0793	2354	18.3	0.3	0.8
*DC-06	45.4362	-113.0799	2342	14.4	0.3	0.6
DC-08	45.4350	-113.0808	2311	17.5	0.3	0.7
DC-10	*45.4345*	*-113.0825*	*2279*	*49.0*	*0.6*	*2.0*
DC-11	45.4297	-113.0791	2241	17.8	0.4	0.8
DC-12	45.4299	-113.0771	2260	18.3	0.3	0.8
DC-13	45.4305	-113.0765	2285	17.4	0.6	0.9
DC-14	45.4313	-113.0755	2298	18.0	0.4	0.8
			(n = 10) avg ± st dev	17.5	1.2	
			LGM (no outliers, n = 9) avg ± st dev	**17.8**	**0.4**	
			Pioneer Mountains ALL Samples (n = 35) median	18.0		
			Pioneer Mountains LGM/Pinedale (n = 22) avg ± st dev	**18.2**	**0.9**	

Exposure ages were calculated using version 3.0 of the Online Exposure Age Calculator (Balco et al., 2008) and the Promontory Point production rate (Lifton et al., 2015) with LSDn scaling. Calculations assumed no erosion, elevation/pressure flag = standard atmosphere, and 07KNSTD.

Italics indicate samples not included in the LGM/Pinedale (30–16 ka) averages

Asterisk (*) indicate possible outliers as identified by the OEAC single landform outlier detection

5. Results and Implications

5.1 Geomorphic landforms and mapping

In each of the three glacial valleys, terminal and/or lateral moraines are prominent topographic features forming latero-frontal ridges (Fig. 4). During the course of our field work, we observed many glacio-geomorphic landforms (e.g., moraines, kettle ponds, hummocky topography, steep U-shaped valley walls, and lateral ridges) and evidence of glacial abrasion (e.g., striations and polish on boulders), quarrying (e.g., roche moutonnée with bouldery till in its lee), deposition of glacial erratics, and post-glacial landslides, rock fall, and slumps along some of the steep-sided moraine crests. Based on these field observations within the study region, few examples of older moraines exist in the east Pioneers, however, we did find one location with exceptionally weathered boulders along a low-relief, sub-rounded moraine in the Canyon Creek terminus zone that produced ages much older than the Pinedale.

Based on the Google Earth satellite imagery and drone-derived aerial orthophotos, we derived maximum glacier extents for Birch Creek (~28 km^2), Canyon Creek (~47 km^2), and Dingley Creek (~4 km^2). In the upper valley and cirque regions where terrain is rugged and access limited (i.e., no roads or trails, extensive blowdown, and/or private land), the satellite imagery provided sufficient resolution to estimate past glacier coverage. The aerial imagery indicates a number of cols along the central and southern portion of East Pioneer spine, where glacial ice may have overridden drainage divides.

5.2 Cosmogenic ^{10}Be exposure ages

Background-corrected sample ^{10}Be concentrations are (3.13 to 41.59) × 10^5 atoms g^{-1} (Table 2), yielding exposure ages of 14.3 ± 0.5 ka to 222.5 ± 2.1 ka (n = 35, 1 SD internal uncertainties, Table 3). Overall, the median exposure age is 18.0 ka, with a broad range of exposure ages that span the pre Bull Lake, penultimate glacial (i.e., Bull Lake), last glacial (i.e., Pinedale), and late glacial. The youngest grouping of exposure ages (14.3–16.0 ka, BC01–06) are from a recessional lateral moraine in the Birch Creek valley, while the oldest exposure ages (90.6, 142.5, 222.5 ka, CC13–15) occur on a rounded, left-lateral, composite moraine indicating multiple prior glacial advances in the Canyon Creek drainage. Samples uniquely indicative of the last glacial maximum extent from well-preserved outer moraines show deglaciation occurring at 18.2 ± 0.9 ka, (n = 22, average, 1 SD). In the following sections, we combine our field observations and calculated exposure ages to create a best estimate for LGM deglaciation timing in each valley.

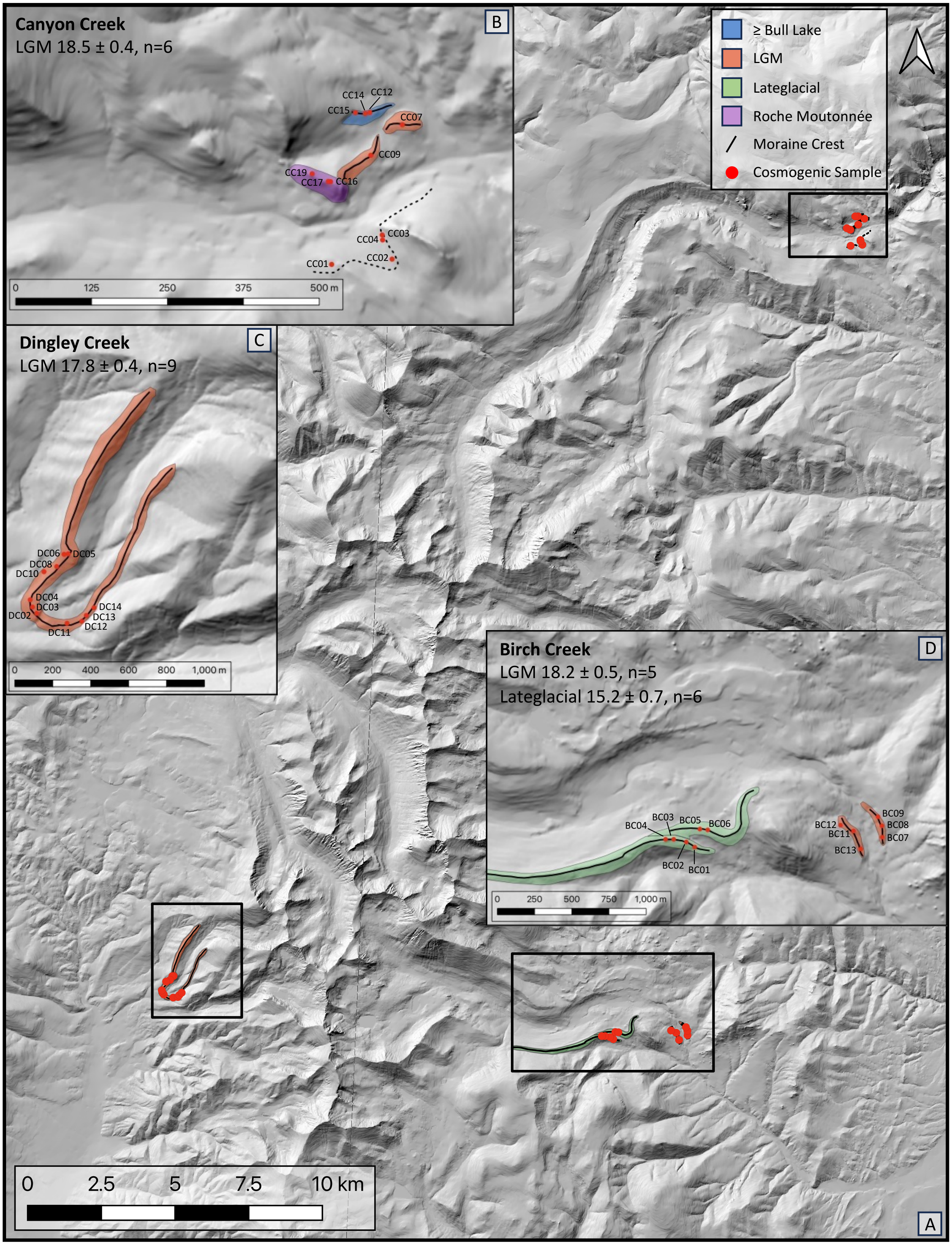
Canyon Creek
LGM 18.5 ± 0.4, n=6
B
CC14
CC12
CC15
CC07
CC09
CC19
CC17
CC16
CC04
CC03
CC02
CC01
0
125
250
375
500 m
≥ Bull Lake
LGM
Lateglacial
Roche Moutonnée
Moraine Crest
Cosmogenic Sample
Dingley Creek
LGM 17.8 ± 0.4, n=9
C
DC06
DC05
DC08
DC10
DC04
DC03
DC02
DC14
DC13
DC12
DC11
0
200
400
600
800
1,000 m
Birch Creek
LGM 18.2 ± 0.5, n=5
Lateglacial 15.2 ± 0.7, n=6
D
BC03
BC05
BC06
BC04
BC02
BC01
BC12
BC11
BC13
BC09
BC08
BC07
0
250
500
750
1,000 m
0
2.5
5
7.5
10 km
A

Figure 4. A) Hillshade-derived image from 10 m LiDAR from the USGS of the Pioneer Mountains showing mapped Last Glacial Maximum (LGM) and late glacial deposits. Cosmogenic samples are shown as red circles (refer to Table 1 for sample names, Figs. 6, 7, 8, 9, and Table 3 for ages). Boxes include LGM/Pinedale averages and 1 SD deviation, excluding outliers. Insets B, C, & D) Same as (A) but close-up view of Canyon Creek, Dingley Creek, and Birch Creek, respectively, showing the moraines and sampling sites, corresponding to the black boxes in (A).

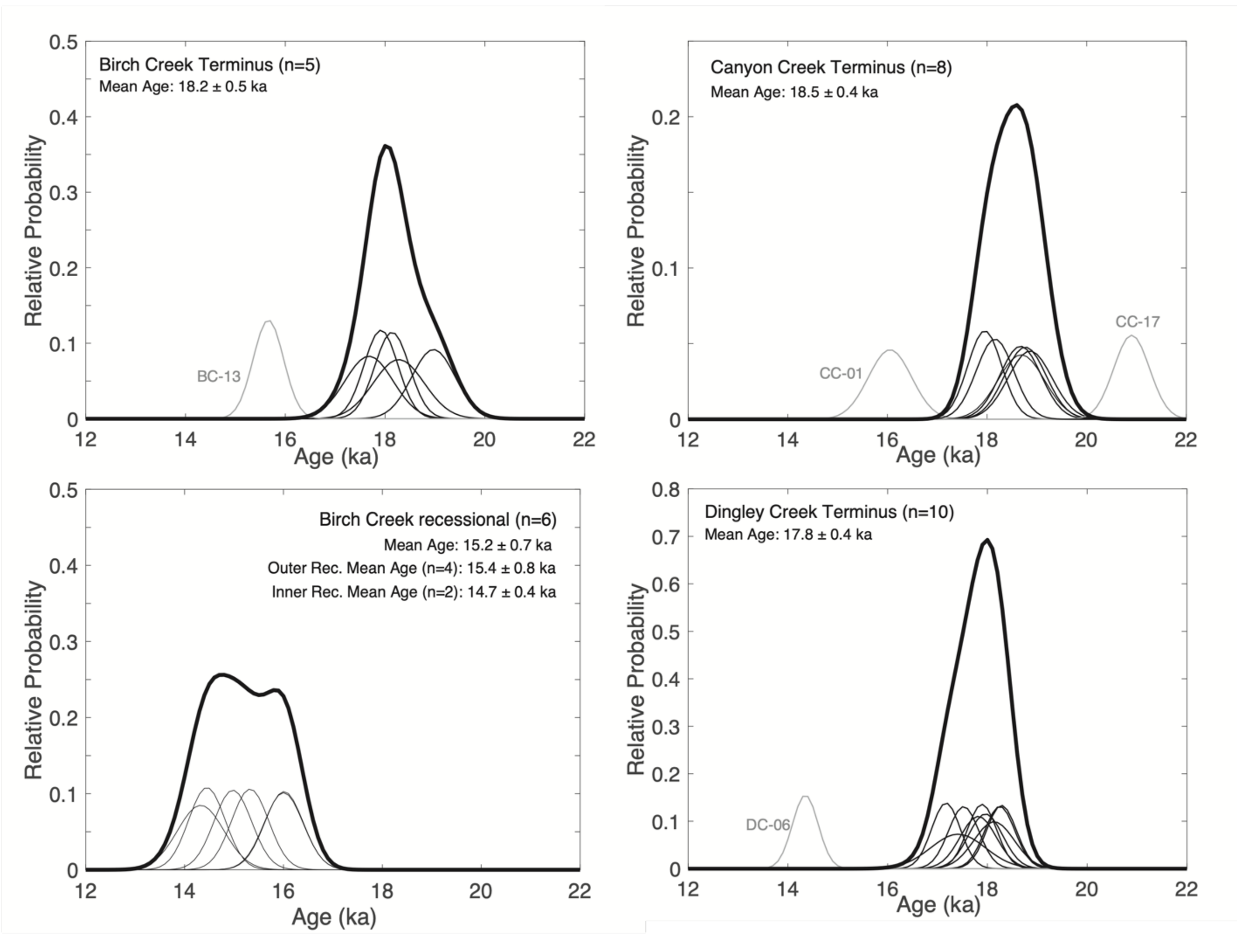

Figure 5. Probability distribution functions of ^{10}Be ages from (top left) Birch Creek terminus, (bottom left) Birch Creek right-lateral recessional, (top right) Canyon Creek terminus, and (bottom right) Dingley Creek terminus. Thin black lines represent individual samples with internal uncertainties, thin grey lines represent individual outliers, and thick black lines show summed probability distributions. The means exclude one Birch Creek boulder (BC13), one Dingley Creek boulder (DC06) and two Canyon Creek boulder outliers (CC01, CC17).

5.2.1 Birch Creek ^{10}Be ages

Six samples from the Birch Creek end moraine yield cosmogenic exposure ages ranging from 15.7 ± 0.3 ka to 19.0 ± 0.4 ka (internal uncertainties, Table 3, Fig. 5). Ages on the end moraine are distributed about a mean age of 17.8 ± 1.1 ka (n = 6, average, 1SD, Table 3, Fig. 5, 6). BC13 yielded a younger age (15.7 ± 0.3 ka, Fig. 6) than the rest, which suggests it had either rolled from the crest or had been fully buried and later exhumed after deposition. Using the OEAC's landform outlier detection, we identified BC13 as a significant outlier (Fig. 5). Excluding BC13, the Birch Creek terminus has a mean exposure age of 18.2 ± 0.5 ka (n = 5, average, 1SD).

Four kilometers up-valley, six boulder samples (BC01–06) from a well-preserved, narrow, right-lateral crest yielded an average exposure age of 15.2 ± 0.7 ka (n = 6). Two of these boulders (BC05 & BC06) were sampled from a nested, inset moraine crest that merged nearby with the ice-distal ridge and yielded an average exposure age of 14.7 ± 0.4 ka (Figs. 4 and 7). The four boulders (BC01–04, 15.4 ± 0.8 ka, n = 4) along the outer moraine crest suggest that despite the boulders' positions, the Birch Creek glacier had receded from its terminus position approximately three thousand years earlier while maintaining its ice thickness at this location. This pattern may be due to the position of a large ridge blocking and constraining the glacier's flow path up-valley of the terminus (e.g., Laabs et al., 2009).

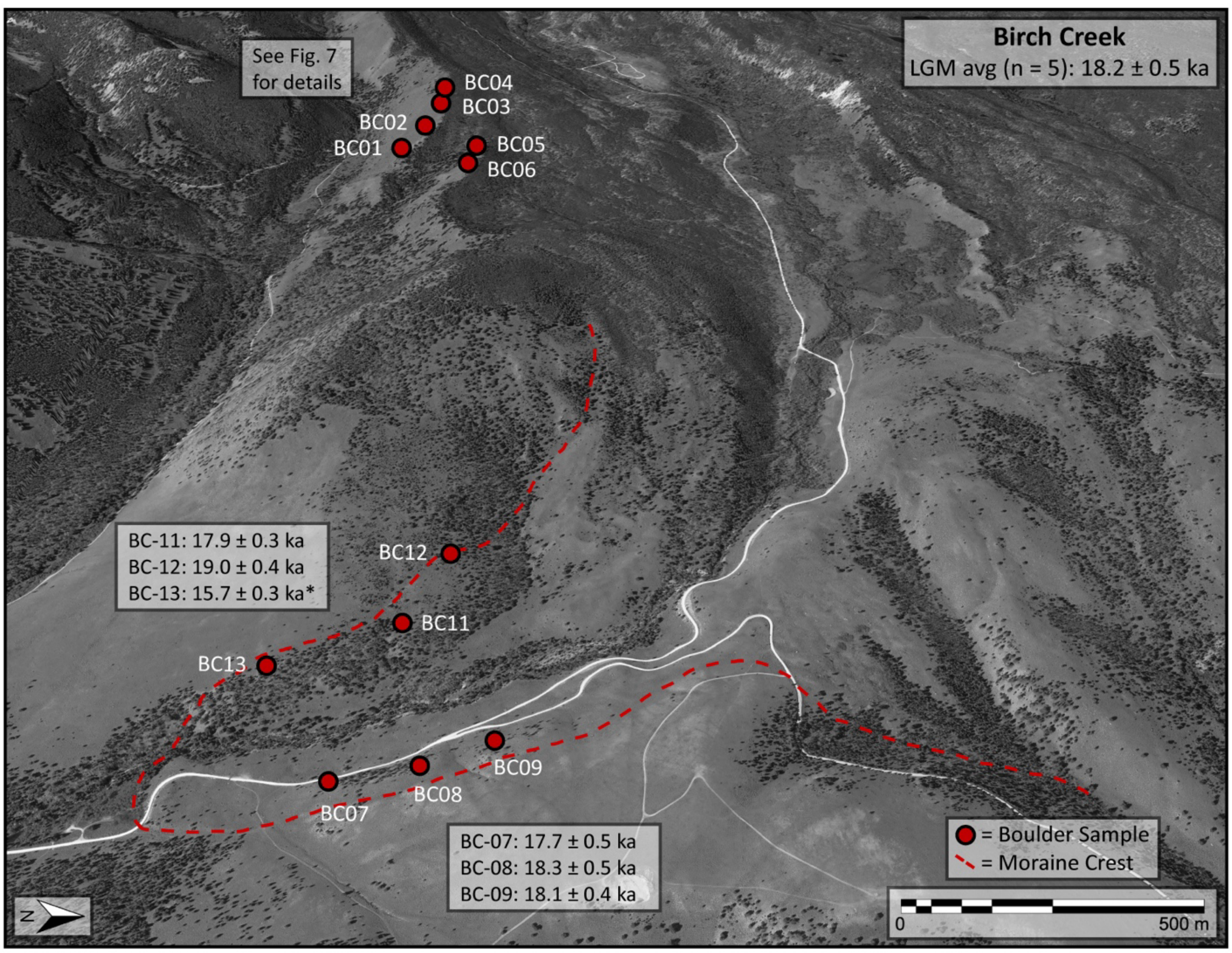

Figure 6. Aerial image of the Birch Creek terminus (Google Earth). Red lines indicate moraine crests/maximum ice extent. Boulder samples were collected from the right and left lateral moraines of the right lobe. Asterisk (*) indicates outlier(s) identified using OEAC single landform outlier detection.

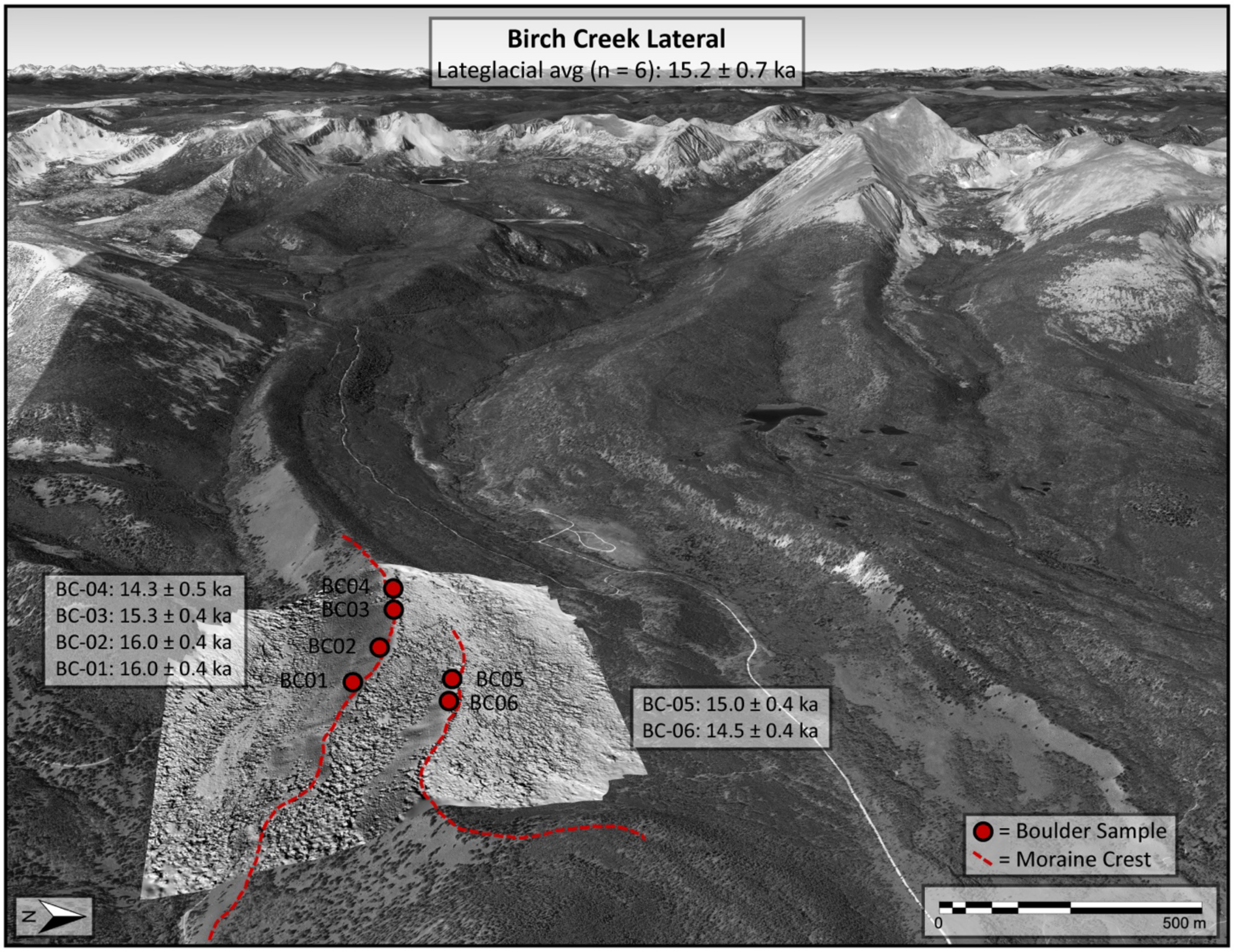

Figure 7. Aerial image (Google Earth) with shaded relief map (from drone survey/photogrammetry) of the Birch Creek right lateral moraine located ~4 km up-valley from the terminus with boulder sample locations (red circles) and ages (boxes). Red lines indicate moraine crests/maximum ice extent.

5.2.2 Dingley Creek ^{10}Be ages

In the Dingley Creek terminus, eleven samples marking the outermost extent yield cosmogenic-exposure ages ranging from 14.4 ± 0.3 ka to 49.0 ± 0.6 ka, with a median age of 17.9 ka (Figs. 5 and 8). Of the eleven exposure ages in Dingley Creek valley, two were identified by CRONUS as outliers. The older outlier, DC10 (49.0 ± 0.6 ka), was a very large boulder (~2 m wide) located ice proximal of the right-lateral moraine crest and appeared to be in place. Based on its geomorphic position, it was likely reworked, with the significantly older age indicative of inheritance of ^{10}Be from a prior period of exposure followed by minimal erosion before deposition. The younger outlier, DC06 (14.4 ± 0.3 ka), was sampled from a lower bench, ice-distal of the steep-sided, right-lateral crest where the moraine bends sharply (Figs. 4 and 8). Although DC06 was located ~10 m below the moraine ridge, it was sampled as a possible older Bull Lake boulder based on its extremely weathered and oxidized appearance. The younger age suggests the boulder was exhumed and rolled from above to the bench. The remaining nine cosmogenic-exposure ages have a mean age of 17.8 ± 0.4 ka (average, 1 SD, Table 3, Figs. 5 and 8), suggesting that glacier ice in Dingley Creek valley persisted at the terminal moraine until this time.

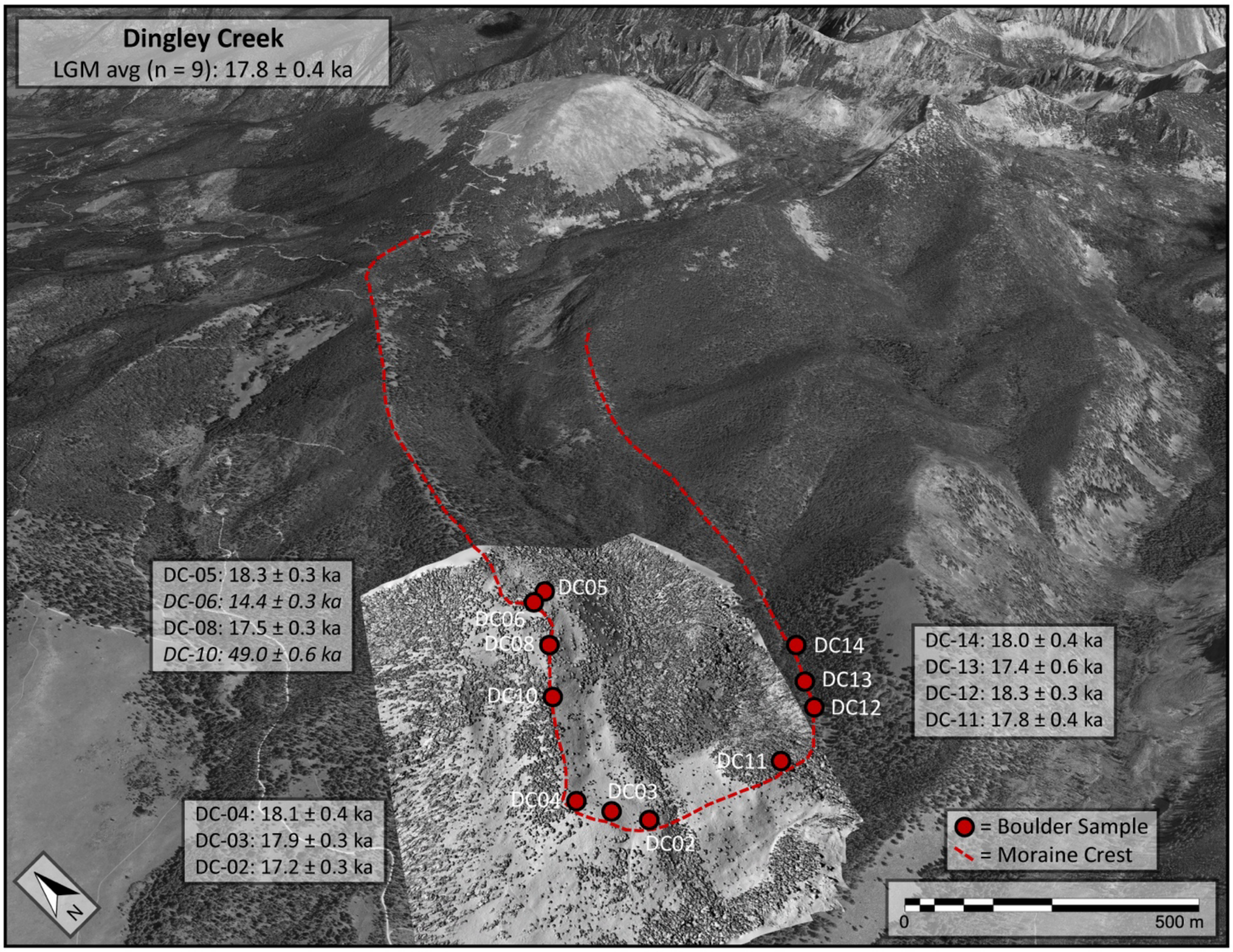

Figure 8. Aerial imagery (Google Earth) with shaded relief map (from drone survey/photogrammetry) of Dingley Creek terminus with boulder sample locations (red circles) and ages (boxes). Red lines indicate moraine crests-maximum ice extent. Italics indicate ages not included in the LGM (30–16 ka) average, asterisk (*) indicates oultiers detected using the OEAC single landform outlier detection.

5.2.3 Canyon Creek ^{10}Be ages

In Canyon Creek valley, a total of 12 boulders were sampled, resulting in a broad range of exposure ages from 16.1 ka to 222.5 ka. A reason for the large spread is that the Canyon Creek terminus area presented an unusual combination of glacial features. These included a lack of an obvious terminal moraine, a broad outwash plain, a right lateral moraine composed of thin till onlapped to a steep bedrock slope, a massive bedrock ridge splitting the drainage, a discontinuous medial moraine with multiple slope failures, and a large, left-lateral moraine entirely absent of granodiorite boulders (Fig. 9). Based on these geomorphic complexities, boulder selection was challenging and produced some unexpectedly old ages, including one likely re-worked with prior exposure (CC02, 68.2 ka, MIS 4) and three (CC13–15) indicating previous glacial advances within the Canyon Creek drainage (discussed in Section 6.3).

LGM boulders from the Canyon Creek terminus yield a range of exposure ages from 16.1 ka to 20.9 ka, with ages uniformly distributed about a mean age of 18.5 ± 1.3 ka (n = 8, average, 1SD, Table 3, Figs. 4, 5, & 9). Of the eight samples, CRONUS identified two outliers, CC01 and CC17 (Fig. 5). CC01 has an exposure age of 16.1 ± 0.4 ka and was sampled from the right-lateral moraine ~0.8 km up valley from the terminus in a small side-valley where ice had bulged outward (Fig. 9). The medium-sized boulder was positioned on the shoulder of a broad, hummocky moraine, but later examination uncovered smaller, partially buried boulders 10–15 m upslope, indicating that the maximum extent was at a higher elevation. Therefore, CC01 likely represents a younger recessional deposit as the glacier thinned and retreated. CC17 has an exposure age of 20.9 ± 0.4 ka; this sample was collected atop the roche moutonnee (Fig. 9), from a large granite boulder perched directly on quartzite bedrock, and may have been exposed earlier while within or on the glacier surface before deposition. After omitting two outliers, the mean age remains 18.5 ka, but yields a narrower standard deviation (0.4 versus 1.3 ka, 1 SD; Table 3).

Older exposure ages on a single outer moraine in the Canyon Creek valley indicate evidence of prior glacial advances in the Pioneer Mountains. The left side of the glacier terminus in Canyon Creek is bounded by a high-sloping ridge, hemming in the northside of the drainage. The broad, left-lateral moraine crest merges with the tertiary-aged surface creating a subtle bench scattered with large quartzite boulders (Figs. 4 and 9); however the resulting data are difficult to interpret due to the large scatter of ages from the moraine. The three boulders all predate the Pinedale (MIS 2), and range in age from pre-Bull Lake to MIS 5b: CC15 (222.5 ± 2.1 ka), CC13 (142.5 ± 1.5 ka), CC14 (90.6 ± 1.1 ka) (Fig. 10).

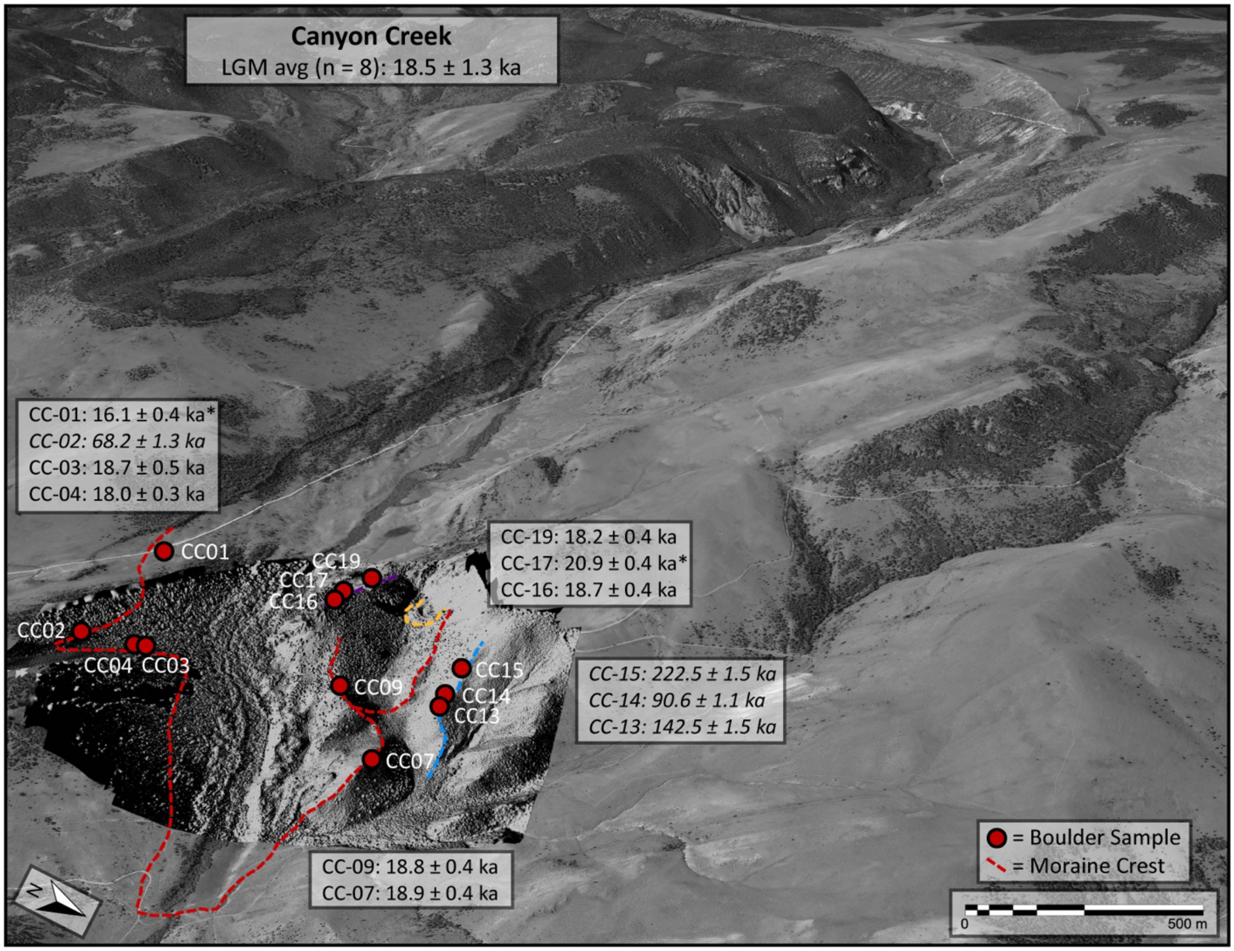

Figure 9. Aerial imagery (Google Earth) with shaded relief map (from drone survey/photogrammetry) of Canyon Creek terminus with boulder sample locations (red circles) and ages (boxes). Red lines indicate maximum Pinedale ice extent, purple line highlights the roche moutonnee, yellow line indicates rock fall atop Pinedale till, and blue line indicates a left-lateral compound moraine of Bull Lake/MIS 7d age. Italics indicate ages not included in the calculation of the LGM (30–16 ka) average, asterisk (*) indicates oultiers detected using the OEAC single landform outlier detection.

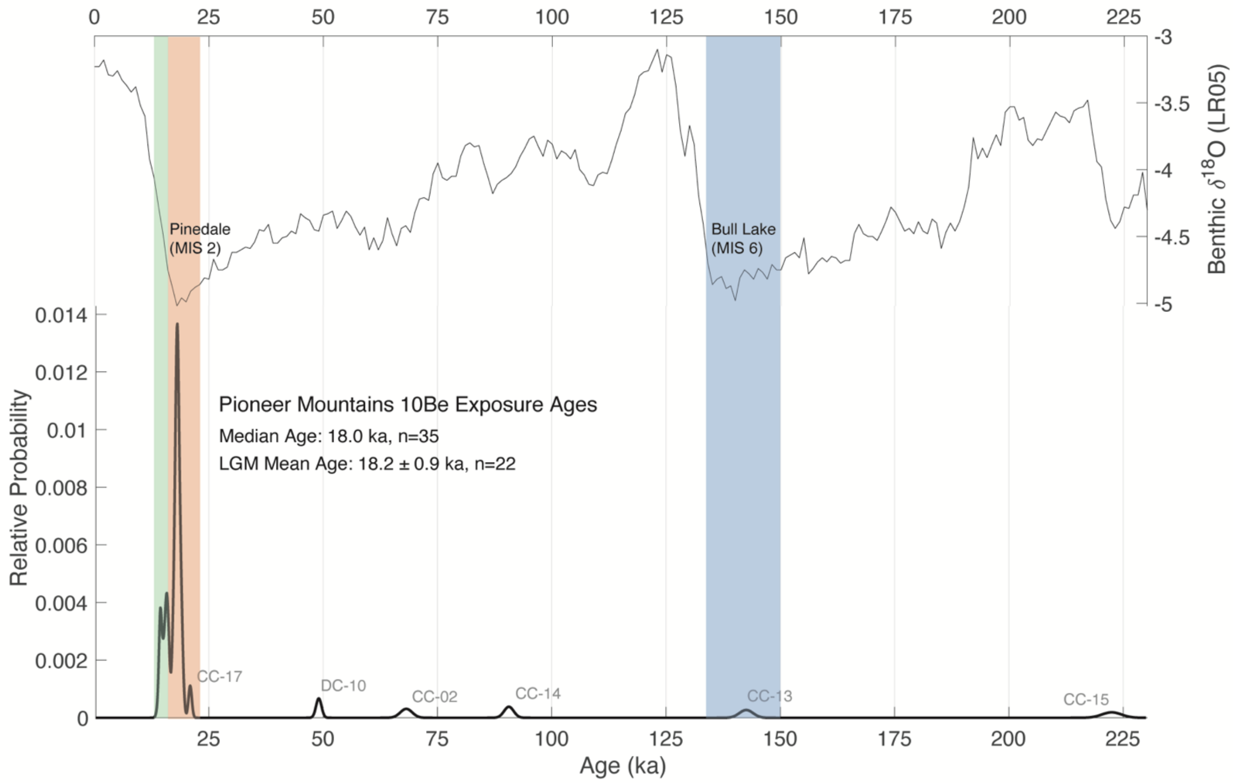

Figure 10. Probability distribution function of ^{10}Be exposure ages from the Pioneer Mountains (lower) with marine benthic δ^{18}O global compilation from *Lisiecki and Raymo (2005)* for comparison to past glacial/interglacial periods (upper). Ages range from pre-Bull Lake to late glacial, with a median age of 18.0 ka (n = 35) and Last Glacial Maximum (LGM 30–16 ka) mean of 18.2 ka (n = 22).

6. Discussion

In the Pioneer Mountains, the maximum Pinedale glacier extent occurred around 18 ka, with all three glacial valleys overlapping in their retreat timing, suggesting a synchronous deglaciation throughout the mountain range. The specific timing of the onset of deglaciation is essential for understanding both the large-scale climatic drivers causing glacier retreat (e.g., insolation, greenhouse gases, albedo, and ocean-atmospheric circulation), as well as the regional factors (e.g., elevation/extent of LIS, locally sourced moisture from pro-glacial lakes, prevailing winds) that influence the spatial pattern of retreat across the northern Rocky Mountains and inland northwest.

6.1 Synchronous LGM glacial retreat among Pioneer Mountain valleys

Compilation of the cosmogenic-exposure ages from all three glacial valleys indicates synchronous timing of maximum glacier extent in the Pioneer Mountains. The individual mean ages for each valley, from the northeast to southwest, are Canyon Creek (18.5 ± 0.4 ka, n = 6), Birch Creek (18.2 ± 0.5 ka, n = 5), and Dingley Creek (17.8 ± 0.4 ka, n = 9), yielding a range-wide average of 18.2 ± 0.9 ka (n = 22). The exposure ages from the different valleys are indistinguishable from one another in their maximum extent timing based on their 1SD age ranges. This overlap indicates that, despite the different orientations (northeast, east, and west-facing) and differing paleo-valley characteristics, the Pioneer Mountain glaciers responded synchronously to the large-scale climatic forces within the resolution of the ^{10}Be chronometer. The consistent timing of moraine abandonment between the three distinct glacier valleys provides confidence that ice retreat among the valleys reflects a broader, regional response, unlike the transient ages derived from the greater Yellowstone glacial system.

6.2 Recessional moraine deposition consistent with Late Pinedale GYGS retreat

Based on the original study design, we had intended on only dating glacial features indicative of maximum extent; however the younger ages determined from boulders along the moraine crest in the Birch Creek Valley were unexpected (Fig. 7). The four exposure ages from the right-lateral outer moraine crest indicate that recession and thinning of the glacier began around 15.4 ± 0.8 ka, which is consistent with recessional ages in the Lewis Range (e.g., Cut Bank Recessional 16.4 ± 0.4 ka) but distinctly younger than initial recession of the northern outlet glacier of the Yellowstone ice cap (e.g., Chico recessional moraine 17.1 ± 0.6 ka).

In general, the Birch Creek recessional ages overlap more closely with the late Pinedale interval of 16–13 ka, as identified in the Greater Yellowstone region by Licciardi and Pierce (2018). During this time period, exposure ages indicate that ice extent on the Beartooth Uplift and Gallatin Range diminished as the Yellowstone ice cap migrated southwest toward the dominant source of moisture, leading to ice advances in the Teton Range (e.g., Jenny Lake Outer, 15.5 ± 0.5 ka) and Jackson Hole region (e.g., Pinedale 2 southern lobe, 15.8 ± 0.8 ka) (Licciardi and Pierce, 2018). The remaining glaciers in the northern GYGS stabilized, depositing the recessional moraines of the Deckard Flats readjustment (15.1 ± 1.2 ka) and Junction Butte (14.9 ± 0.4 ka) terminus (Licciardi and Pierce, 2018). The timing of the Birch Creek recession appears to overlap broadly with the draining and cessation of Glacial Lake Missoula after 15.6 ka (Dyke et al., 2003) and aligns with other down-valley recessional moraine ages in the northern and central Rocky Mountains (see Table 3 of Laabs et al., 2020).

6.3 Bull Lake and pre-Bull Lake ages indicate previous glacial advances

The significantly older exposure ages in Canyon Creek valley suggest evidence of prior glacial advances in the Pioneer Mountains. Three boulders from the outer left-lateral moraine range in age from pre-Bull Lake (MIS 7d, 225 ka) to MIS 5b (87 ka, Figs. 9 and 10). The outermost, left-lateral moraine has none of the granodiorite boulders common to the Pinedale-aged landforms, many of the quartzite boulders show signs of frost shattering, the moraine morphology is relatively smooth, and the ages are all appreciably older than the LGM, all of which suggest the moraine may have been occupied during multiple previous glaciations. After determination of the boulder ages, a follow-up field effort identified a much smaller moraine in the lower portion of the narrower, left valley that had initially been mapped as a recessional moraine. The moraine contained similarly appearing granodiorites as the other Pinedale-age glacial features, thus presenting a much reduced Pinedale maximum extent compared to the higher Bull Lake moraine (crest located 25–35 m above Pinedale left-lateral moraine, Fig. 9). These exposure ages are the only dated evidence of prior glaciations in the Pioneer Mountains, and from our field observations throughout the range, few examples of older moraines exist in the eastern glacial valleys.

Bull Lake-aged moraines in alpine glacial systems are generally sparse in the western US compared to Pinedale moraines, and where present are typically ~10% greater in maximum extent than the Pinedale, suggesting that the penultimate glaciation was either cooler or wetter (Blackwelder, 1915; Licciardi and Pierce, 2018; Pierce, 2003). One caveat is that the up-valley morphology and hypsometry of glacial valleys during the Bull Lake is unknown, complicating the interpretations of relative glacier lengths between the two glacial periods (e.g., Anderson et al., 2012). In many northern Rocky Mountain locales, the Pinedale glacial extents have overridden the Bull Lake ice advances, and reworked the till, thus erasing any prior evidence of their presence. Moreover, the remaining evidence for Bull Lake glacial extents is generally more degraded by surface processes, being an order of magnitude older than fresher Pinedale features. Finding a relatively well-preserved composite moraine of Bull Lake age in the northeast aspect of the Pioneer Mountains is in line with other occurrences of Bull Lake-aged moraines, which tend to be preserved along north and northeast aspects of the northern Rocky Mountains (e.g., Beartooth Uplift) (Licciardi and Pierce, 2018, 2008; Pierce, 2003).

6.4 Pioneer Mountain glacier maxima younger than global and regional LGM

The maximum Pinedale glacier extents of the Pioneer Mountains (18.2 ± 0.9 ka, n = 22, avg., 1SD) may be younger than the global LGM (21 ± 2 ka, Peltier and Fairbanks, 2006). The timing of initial moraine abandonment in the Pioneer Mountains is relatively young compared to most other northern Rocky Mountain ranges (e.g., average of old modes for the Wind River/Big Horn Mountains: 22.4 ± 1.7 ka, n = 8, 1SD) and Columbia Plateau (e.g., old mode of the Wallowa Mountains: 22.8 ± 0.8 ka, n = 9, 1SD, Table 4, Fig. 11). The timing of maximum glacier extents of the Pioneer Mountains are more similar to the alpine and outlet glaciers of the northwestern greater Yellowstone glacial system (17.8 ± 1.1 ka, n = 24, (Laabs et al., 2020; Licciardi et al., 2001; Licciardi and Pierce, 2008; Quirk et al., 2022), and the Lewis Range (17.2 ± 0.6 ka, n = 7, 1 SD, Quirk et al., 2022) which are approximately five-hundred to one thousand years younger than the Pioneer Mountains and overlap within their 1 SD ranges. Proceeding the early onset of deglaciation (i.e., old mode), there is a second period of near-maximum extents within the terminal moraine complexes of the Wallowa, Big Horn, and Wind River Mountains, which are known as the “young” mode (18.3 ± 1.0 ka, n = 11), Table 4. This similar timing of both maximum and near-terminal extents occurring region wide at ~18 ka signals a consistent response to a broader climate forcing, and the later deglaciation timing is closely aligned with the timing of global patterns of change (e.g., atmospheric CO_2 increase, northern-hemisphere ice-sheet area decline, and strengthened snow-albedo feedback: see Shakun et al., 2012, Fig. 3).

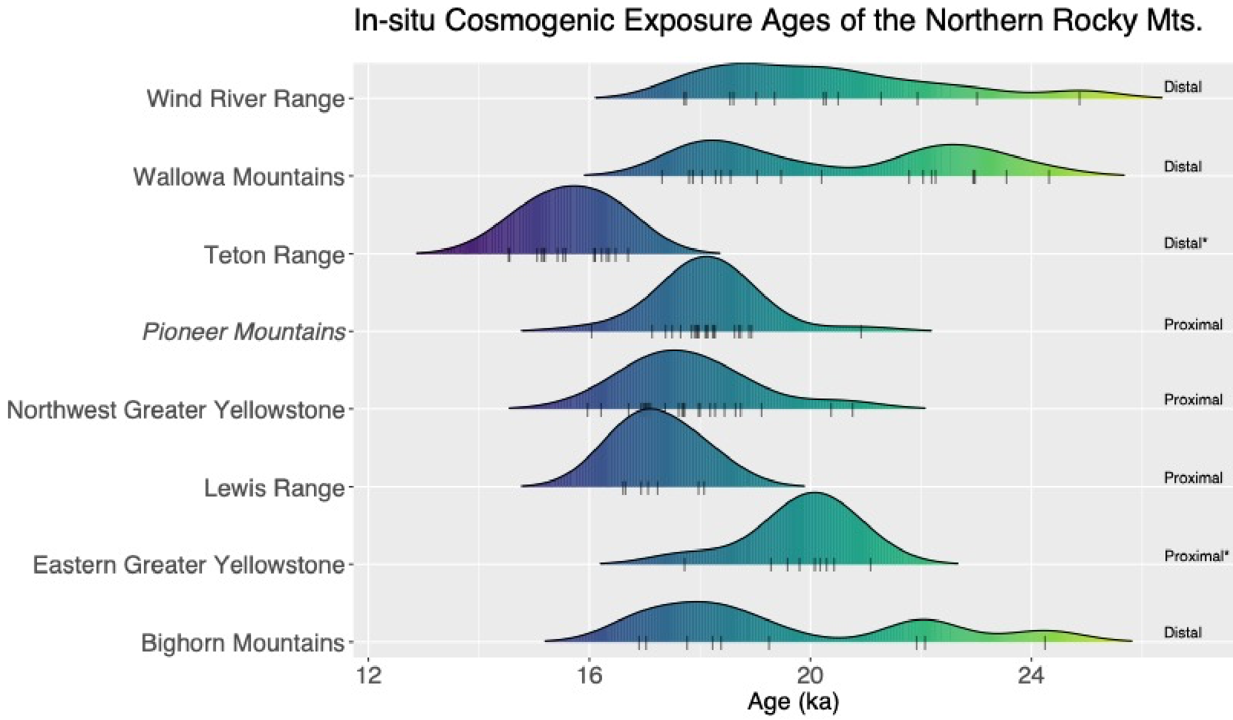

Figure 11. Probability density function comparison of the last glaciation (MIS 2) ages of the Wind River Range, Wallowa Mountains, Teton Range, Pioneer Mountains, Northern and Eastern GYGS, and Bighorn Mountains. The color gradient shows the ages from dark blue (youngest) to yellow (oldest). Ranges are labeled as proximal or distal to the LIS margin, and * indicates sites that were partially impacted by the migrating position of the Yellowstone Ice Cap. Compiled using code in R-Studio shared by Jordan Dahle.

Table 4

Northwest/Northern Rocky Mountain region Last Glacial Maximum exposure ages

Sample name/locality by N-S proximity to LIS	Moraine Type/Number of ages	Original Source	^{10}Be Exposure Age (ka)[a]	^{10}Be Internal Uncertainty (ka)[a]
Lewis Range, Glacier National Park, MT				
Cut Bank Creek	terminal moraine, n = 7	Quirk et al. 2022	17.2	0.6
Cut Bank Creek	recessional moraine, n = 3	Quirk et al. 2022	16.4	0.4
Northwestern Greater Yellowstone Glacial System, MT/WY				
Eightmile, GYGS, MT	terminal moraine, northern Yellowstone outlet glacier, n = 11	Licciardi et al. 2001	17.9	1.2
Pine Creek, Absaroka Range, MT	terminal and lateral moraines, n = 7	Licciardi & Pierce, 2008	18.2	1.3
South Fork Deep Creek, Absaroka Range, MT	left lateral moraine, n = 3	Laabs et al. 2020	17.5	1.1
Cascade Creek, Absaroka Range, MT	scoured bedrock, n = 2	Laabs et al. 2020	16.9	0.2
Gallatin River Valley, Gallatin Range, WY	terminal moraine, n = 1	Licciardi & Pierce, 2008	17.7	0.4
		avg ± st dev (n=24)	**17.8**	**1.1**
Pioneer Mountains, MT				
Birch Creek	terminal moraine, n = 5	This Study	18.2	0.5
Canyon Creek	terminal moraine, n = 6	This Study	18.5	0.4
Dingley Creek	terminal moraine, n = 9	This Study	17.8	0.4
		avg ± st dev (n=22)	**18.2**	**0.9**
Birch Creek	recessional moraine, n = 6	This Study	15.2	0.7
Eastern Greater Yellowstone Glacial System, MT/WY				
Clarks Fork, WY	terminal moraine, n = 9	Licciardi & Pierce, 2008	19.8	0.9
Wallowa Mountains, OR				
Wallowa Lake Old Mode	multi-crested terminal moraine complex, n = 9	Licciardi et al. 2004	22.8	0.8
Wallowa Lake Young Mode	multi-crested terminal moraine complex, n = 10	Licciardi et al. 2004	18.5	0.8
Teton Range, WY				
Hendricks Pond (Pinedale 2- southern lobe)	southern terminal of Snake River lobe, n = 5	Licciardi & Pierce, 2008	15.8	0.8
Cascade Canyon/Jenny Lake Outer	broad terminal complex impounding Jenny Lake on east side of range, n = 11	Licciardi & Pierce, 2018	15.5	0.5
		avg ± st dev (n=16)	**15.7**	**0.7**
Wind River/Bighorn, WY Old Mode				
Wind River, Bull Lake, Pinedale 2, 36Cl	terminal moraine complex-middle moraine, n = 3	Phillips et al. 1997	22.4	2.8
Wind River, North Fork, Popo Agie Basin	terminal moraine, n = 2	Dahms et al. 2018	21.7	0.5

Bighorn, North Fork Clear Creek Canyon	terminal, oldest grouping, n = 3	Laabs et al. 2020	22.8	1.3
		avg ± st dev (n=8)	**22.4**	**1.7**
Wind River/Bighorn, WY Young Mode				
Wind River, Bull Lake, Pinedale3 PN3, 36Cl	terminal moraine complex-inner moraine, n = 3	Phillips et al. 1997	18.9	1.2
Wind River, Sinks Canyon 2, Popo Agie Basin	recessional moraine ~few km up-valley, inner, n = 2	Dahms et al. 2018	18.4	0.9
Bighorn, North Fork Clear Creek Canyon	terminal moraine, intermediate grouping, n = 3	Laabs et al. 2020	18.0	1.1
Bighorn, Tensleep Canyon	terminal moraine, n = 3	Laabs et al. 2020	17.9	1.8
		avg ± st dev (n=11)	**18.3**	**1.0**

[a] All recalculated ages from Laabs et al., 2020 using Version 3 of the Online Exposure Age Calculator (Balco et al., 2008) and the Promontory Point production rate (Lifton et al., 2015) with LSDn scaling, Std atmosphere, zero erosion rate, and available on Ice-D Alpine

6.5 Differences in regional deglaciation history and climate impacts

Differences in the regional spatial pattern of deglaciation onset timing are apparent, based on the relatively young ages from the Pioneer Mountains, northwestern GYGS, and Lewis Range, and the older ages to the west (e.g., Wallowa Mountains) and east (Big Horn Mountains) of the northern Rocky Mountain cordillera (Fig. 11). Prior explanation for the relatively younger deglacial timing of the northwestern GYGS focused on the migrating center of the Yellowstone ice cap, which influenced the timing of outlet glaciers as the divide progressed southwestward from self-sustaining orographic precipitation (Licciardi and Pierce, 2018). Our findings from the Pioneer Mountains, in concert with the northwestern GYGS and Lewis Range, suggest that the relatively young timing of deglaciation was not solely related to the migrating ice cap, but to regional climate conditions that impacted the ranges proximal to the LIS. The question then arises, why do the Pioneer Mountains, northwestern GYGS, and Lewis Range have younger maximum glacial extents, and why do they not record a similar response to the initial summer insolation forcing like the Wallowa, Big Horn, and Wind River Mountains between 23–22 ka?

6.5.1 Ice-sheet driven shifts in atmospheric circulation and timing of northern Rocky Mountain glacier maxima

A prevailing hypothesis in previous work (Alder and Hostetler, 2015; Hostetler and Clark, 1997; Licciardi et al., 2004; Thackray, 2008) is that the retreat of North American ice sheets (i.e., Cordilleran and Laurentide) and the accompanying northward shift of the jet stream resulted in increased precipitation, allowing glaciers to persist at or re-advance to their maximum extents in the northern Rocky Mountains. Licciardi et al. (2004) and Thackray et al. (2004) have attributed the relatively late maxima of glaciers in the region to increased moisture availability after 21 ka induced by retreat of the LIS. They proposed that precipitation controls on glacier mass balance were substantial and that regional-scale climate change was important in determining the timing of the start of ice retreat in ranges of the Rocky Mountains.

This explanation has been more recently investigated by Oster et al., (2015), who compiled an ensemble of general circulation model (GCM) experiments from the Paleoclimate Modeling Intercomparison Project (PMIP2 and PMIP3, Braconnot et al., 2012, 2007) that incorporated the North American ice sheet to simulate past shifts in climatic conditions during the LGM: 21 ka. The majority of the climate models analyzed showed agreement between the simulated conditions and the precipitation-sensitive proxy records from western North America. In general, the model-proxy data agreement indicated dryer than modern conditions in the Pacific Northwest and wetter than modern conditions in the Southwest, but with some mismatch in the central Rocky Mountains (Oster et al., 2015). This north-to-south LGM precipitation dipole formed due to the North American ice sheets causing a southward shift in the winter storm track and a strengthened jet related to squeezing by high pressure systems (Bartlein et al., 1998; Harrison et al., 2013; Hudson et al., 2019; Lora, 2018; Lora and Ibarra, 2019; Oster et al., 2015)

Some of the limitations of the migrating jet-stream hypothesis are related to the timing and extent of the northward shift as the LIS began its retreat after ~21 ka. Transient and time-slice GCM simulations of the LGM (e.g., Transient Climate Evolution of the past 21 kyr experiments: TraCE 21, Liu et al., 2009 and Paleoclimate Model Intercomparison Project: PMIP3, Braconnot et al., 2012) that incorporate variations of North American ice sheet orography based on reconstructions (e.g., ICE-5G, Peltier, 2004) indicate that Northern Hemisphere annual temperatures remained low throughout the LGM, and then relatively rapid warming beginning at ~17 ka and continuing until 14.5 ka (Clark et al., 2012; He et al., 2013; Liu et al., 2009; Shakun et al., 2012). Tulenko et al. (2020) utilized the TraCE 21 simulations to investigate the impact of the LIS on the temperature and precipitation patterns in the western US and find that although annual temperatures began increasing at ~17.5 ka, both winter and summer precipitation continued to decrease between 19–17 ka, with winter precipitation not increasing until around 16 ka and summer precipitation not increasing until ~14 ka (see Fig. 3 E & G in Tulenko et al., 2020).

These simulations are inconsistent with the proposed winter jet-stream migration causing increases in precipitation in the northern Rocky Mountains at the 19–17 ka interval, leading to later advances of northern glaciers. In addition, proxy records and glacier extent from the central Rocky Mountains indicate the mean position of the winter jet remained shifted southward based on the prolonged high-stand of pluvial Lake Bonneville, UT until ~16 ka (Laabs et al., 2009), and is also supported by the younger near-LGM glacier dimensions observed in the central Rocky Mountains (e.g., Wasatch—Bells Canyon, 16.7 ka and Lake Fork, 16.8 ka, Ruby Mountains—Seitz Canyon 4-7, 16.7 ka, Sangre de Cristo—Willow Creek, 15.7 ka, Sawatch Range, 15.5–17.2 ka, and Teton Range—Jenny Lake Outer/Hendrick Pond, 15.7 ka, see Laabs et al., 2020 for ages). The pattern of higher precipitation sustaining pluvial lakes and near-maximum glacier extents in the central Rocky Mountains until 17–16 ka, consistent with the TraCE results, point to a later northward return of the jet-stream.

It remains plausible that a northward migration of an expanded jet stream would be broad enough to increase precipitation in both the central and northern Rocky Mountains concurrently (e.g., Quirk et al., 2020), allowing glaciers to maintain near-terminal extents in the Wasatch and Ruby Mountains while increasing even more further north, resulting in the late local LGM observed in the northern Rocky Mountain records (Quirk et al., 2020b). Based on the existing glacier chronologies, we are unable to exclude this latter scenario, but the GCM simulations generally produce a squeezed, strengthened jet-stream during the LGM, incompatible with a wider zonal flow (Hudson et al., 2019; Lora and Ibarra, 2019; Oster et al., 2015).

6.5.2 Glacier maxima sustained by ice-sheet proximity

As an alternative to some of the shortcomings with the migrating jet-stream hypothesis, we propose that the glacier mass balances and extents were maintained due to the Pioneer Mountains and northern GYGS proximity to the Laurentide Ice Sheet (Fig. 1). This could be achieved in a number of ways, including cold, katabatic winds that descended off the ice sheet reducing melting and a greater contribution of precipitation offsetting ablation (Bartlein et al., 1998; Hudson et al., 2019; Lora and Ibarra, 2019; Oster et al., 2015; Wong et al., 2016). In simulations of the last glacial period, the presence of the LIS produced its own high pressure system with anticyclonic winds, prevailing from the north/northeast along the ice sheet margin in northern ID/MT (Oster et al., 2015, see Fig. 1 in Putnam, 2015). Additionally, it is possible that locally derived precipitation from extensive pro-glacial meltwater lakes along the LIS margin provided extra precipitation, thus increasing glacier mass balance and prolonging glacier extents (e.g., Laabs et al., 2009; Munroe et al., 2006; Munroe and Mickelson, 2002). North of the Pioneer Mountains, radiocarbon ages from paleo-shorelines indicate initial meltwater filling of Glacial Lake Missoula (~3,000 square miles, ~2x the modern Great Salt Lake) after 20.8 ka along the ice margin (Dyke, 2004; Dyke et al., 2003), and as the LIS receded continual meltwater production formed numerous pro-glacial lakes (including Glacial Lakes Missoula, Great Falls, and Mussellshell located to the north/northeast of the Pioneer Mountains and GYGS, Fig. 1). A comparable scenario was discussed by Laabs et al. (2009), where the glacier maxima in the western Uinta Mountains was likely sustained by nearby, pluvial Lake Bonneville (~100 km to the west), maintaining glaciers until 4–5 kyr after the global LGM (21 ± 2 cal. ka, Peltier and

Fairbanks, 2006). As the LIS margin retreated further northward throughout the deglaciation and meltwater production decreased and then ceased, we expect that the central Montana pro-glacial lakes drained, eventually eliminating the extra moisture source feeding glaciers in the Pioneer Mountains and other ice-proximal ranges. The youngest paleo-shoreline radiocarbon ages indicate Glacial Lake Missoula was greatly reduced after 15.6 ka (Dyke et al., 2003), which closely overlaps with the timing of the recessional moraines in Birch Creek Valley and the northern GYGS. No age constraints exist for when Glacial Lakes Great Falls and Musselshell drained but based on reconstructions of the retreat of the LIS margin the pro-glacial lakes would have shifted further northward tracking the recession (Dyke et al., 2003; Fullerton et al., 2004).

If the presence of pro-glacial meltwater lakes northward of the Pioneer Mountains and GYGS significantly impacted glacier mass balance, thereby sustaining glacier maxima later than in the Wallowas and Wind Rivers/Big Horns, it may have done so in a number of ways. For example, the presence of a large glacial lake, or series of lakes, along the ice margin may have induced "lake-effect" precipitation, enhancing snow accumulation in areas downwind of the margin from the hypothesized/model-simulated katabatic winds, including ranges in its lee like the Absaroka and Gallatin of the GYGS to the south and the Tobacco Root and Pioneer Mountains to the southwest (Figs. 1 & 2). In addition, reduced glacier ablation may have been caused by decreased melt-season temperatures or increased cloudiness in adjacent areas, similar to effects of the modern Great Lakes (Changnon and Jones, 1972). Due to their more distal location from the ice margin (~300 km: Wallowas; >350 km: Big Horns/Wind Rivers), and lack of large glacial lakes upwind (i.e., north/northeast of the Big Horn and Wind River Mountains), it is possible these ranges did not receive substantial "lake-effect" precipitation and therefore commenced earlier deglaciation following the N.H. summer insolation forcing.

7. Conclusion

Based on the in-situ cosmogenic ^{10}Be exposure ages, as well as field observations of moraine morphology, the maximum extent of the last glaciation in the Pioneer Mountains occurred during the Pinedale (MIS 2) at about 18 ka. The start of ice retreat in the Pioneer Mountains, GYGS, and Lewis Range was delayed until after the global LGM (21 ka) and occurred 3–4 kyr after the onset of deglaciation in the Wallowa Mountains to the west and the Big Horn and Wind River Mountains to the east and southeast, respectively. Glaciers in the Pioneer Mountains began retreating in phase with glaciers in the northwestern greater Yellowstone glacial system and were approximately synchronous with the deglacial timing of near-terminal extents in the Wallowa, Wind River, and Big Horn Mountains, suggesting a coherent, region-wide response to climate forcings driven by increases in global CO_2 concentrations, Northern Hemisphere summer insolation, snow-albedo feedbacks, and ice sheet orography at ~18 ka.

Within the northern Rocky Mountain cordillera, it appears that topography more proximal to the LIS margin maintained full ice extent longer than glaciers further west and east. We propose that glacier extents of the Pioneer Mountains, Lewis Range, and northwestern GYGS persisted at their maxima until ~18 ka due to localized temperature and precipitation impacts from the ice sheet's presence. Anticyclonic winds over the continent-wide ice sheet would have produced cold, katabatic winds that may have reduced summer melting and transported glacial-lake derived moisture, potentially offsetting ablation and sustaining the ice proximal glaciers. In contrast, northern glaciers located further from the ice sheet margin and associated meltwater lakes retreated earlier, most likely due to increases in summer air temperature and continuing reductions in summer precipitation following the global LGM (e.g., Tulenko et al., 2020). A compilation of precipitation-sensitive proxy records from the western US supports the likelihood that the LIS forced an equatorward hydroclimate shift in western North America, resulting in reduced precipitation in the interior northwestern US during the LGM (Oster et al., 2015), and likely persisted into the post-glacial interval (~21–18 ka) when air temperatures began to rise (Tulenko et al., 2020). Thus, the contrast between relatively dry climate conditions in the northwestern US and enhanced moisture availability along certain sections of the ice sheet margin as lakes developed, may explain the timing differences in glacier maxima between the more distal Wallowa, Wind River, and Big Horn Mountains compared to the more proximal Pioneer Mountains, northwestern GYGS, and Lewis Range.

Acknowledgements

We thank Marc Caffee for prompt and meticulous measurement of ^{10}Be at PRIME: Jesse Mosolf for use of laboratory facilities at Montana Tech; Jason Drebber for help with sample preparation; Ben Laabs for permission to use a modified version of his Western U.S. topographic/ice extent map in Fig.1; Jordan Dahle for providing her age compilation script (R-Studio) for the ridgeline plots. The manuscript was improved by informal conversations with

Eric Leonard. This work was funded by NSF-EAR 2018222 to S. Schoenemann and NSF-EAR 2018059 to L. Corbett and P. Bierman as well as NSF-EAR 1735676 that supported laboratory analysis. Additional support provided by the MT EPSCoR.

Data Availability

The Pioneer Mountain cosmogenic exposure ages will be made available on the ICE-D: Alpine website: https://version2.ice-d.org/alpine/ and the Northern Rocky Mountain individual ages used in Table 4/Figure 11 will be provided as a supplementary Excel data table per request.

References

Alden, W.C., 1953. Physiography and glacial geology of western Montana and adjacent areas. U.S. Geological Survey Professional Paper 231 200.

Alder, J.R., Hostetler, S.W., 2015. Global climate simulations at 3000-year intervals for the last 21 000 years with the GENMOM coupled atmosphere–ocean model. Clim. Past 11, 449–471. https://doi.org/10.5194/cp-11-449-2015

Balco, G., 2011. Contributions and unrealized potential contributions of cosmogenic-nuclide exposure dating to glacier chronology, 1990-2010. Quat. Sci. Rev. 30, 3–27. https://doi.org/10.1016/j.quascirev.2010.11.003

Balco, G., Stone, J.O., Lifton, N.A., Dunai, T.J., 2008. A complete and easily accessible means of calculating surface exposure ages or erosion rates from 10Be and 26Al measurements. Quaternary Geochronology 3, 174–195. https://doi.org/10.1016/j.quageo.2007.12.001

Bartlein, P.J., Anderson, K.H., Anderson, P.M., Edwards, M.E., Mock, C.J., Thompson, R.S., Webb, R.S., III, T.W., Whitlock, C., 1998. Paleoclimate simulations for North America over the past 21,000 years: features of the simulated climate and comparisons with paleoenvironmental data. Quat. Sci. Rev. 17, 549–585. https://doi.org/10.1016/s0277-3791(98)00012-2

Bierman, P.R., 1994. Using in situ produced cosmogenic isotopes to estimate rates of landscape evolution: A review from the geomorphic perspective. J. Geophys. Res.: Solid Earth 99, 13885–13896. https://doi.org/10.1029/94jb00459

Blackwelder, E., 1915. Post-cretaceous history of the mountains of western Wyoming. J. Geol. 23, 302–340.

Borchers, B., Marrero, S., Balco, G., Caffee, M., Goehring, B., Lifton, N., Nishiizumi, K., Phillips, F., Schaefer, J., Stone, J., 2016. Geological calibration of spallation production rates in the CRONUS-Earth project. Quat. Geochronol. 31, 188–198. https://doi.org/10.1016/j.quageo.2015.01.009

Braconnot, P., Harrison, S.P., Kageyama, M., Bartlein, P.J., Masson-Delmotte, V., Abe-Ouchi, A., Otto-Bliesner, B., Zhao, Y., 2012. Evaluation of climate models using palaeoclimatic data. Nat. Clim. Change. 2, 417–424. https://doi.org/10.1038/nclimate1456

Braconnot, P., Otto-Bliesner, B., Harrison, S., Joussaume, S., Peterchmitt, J.-Y., Abe-Ouchi, A., Crucifix, M., Driesschaert, E., Fichefet, Th., Hewitt, C.D., Kageyama, M., Kitoh, A., Laîné, A., Loutre, M.-F., Marti, O., Merkel, U., Ramstein, G., Valdes, P., Weber, S.L., Yu, Y., Zhao, Y., 2007. Results of PMIP2 coupled simulations of the Mid-Holocene and Last Glacial Maximum; Part 1: experiments and large-scale features. Clim. Past. 3, 261–277. https://doi.org/10.5194/cp-3-261-2007

Briner, J.P., Goehring, B.M., Mangerud, J., Svendsen, J.I., 2016. The deep accumulation of 10Be at Utsira, southwestern Norway: Implications for cosmogenic nuclide exposure dating in peripheral ice sheet landscapes. Geophys. Res. Lett. 43, 9121–9129. https://doi.org/10.1002/2016gl070100

Brugger, K.A., 2007. Cosmogenic 10Be and 36Cl ages from Late Pleistocene terminal moraine complexes in the Taylor River drainage basin, central Colorado, USA. Quat. Sci. Rev. 26, 494–499. https://doi.org/10.1016/j.quascirev.2006.09.006

Brugger, K.A., Laabs, B., Reimers, A., Bensen, N., 2019a. Late Pleistocene glaciation in the Mosquito Range, Colorado, USA: chronology and climate. J. Quat. Sci. 34, 187–202. https://doi.org/10.1002/jqs.3090

Brugger, K.A., Ruleman, C.A., Caffee, M.W., Mason, C.C., 2019b. Climate during the Last Glacial Maximum in the Northern Sawatch Range, Colorado, USA. Quaternary 2, 36. https://doi.org/10.3390/quat2040036

Changnon, S.A., Jones, D.M.A., 1972. Review of the influences of the Great Lakes on weather. Water Resour. Res. 8, 360–371. https://doi.org/10.1029/wr008i002p00360

Clark, P.U., Shakun, J.D., Baker, P.A., Bartlein, P.J., Brewer, S., Brook, E.J., Carlson, A.E., Cheng, H., Kaufman, D.S., Liu, Z., 2012. Global climate evolution during the last deglaciation. Proc. Natl. Acad. Sci. U.S.A 109, E1134–E1142. https://doi.org/10.1073/pnas.1116619109/-/dcsupplemental/appendix.pdf

Corbett, L.B., Bierman, P.R., Rood, D.H., 2016. An approach for optimizing in situ cosmogenic 10Be sample preparation. Quaternary Geochronology 33, 24–34. https://doi.org/10.1016/j.quageo.2016.02.001

Dahms, D., Egli, M., Fabel, D., Harbor, J., Brandová, D., Portes, R. de C., Christl, M., 2018. Revised Quaternary glacial succession and post-LGM recession, southern Wind River Range, Wyoming, USA. Quat. Sci. Rev. 192, 167–184. https://doi.org/10.1016/j.quascirev.2018.05.020

Dahms, D.E., Birkeland, P.W., Shroba, R.R., Miller, C.D., 2010. Latest Quaternary glacial and periglacial stratigraphy, Wind River Range, Wyoming. The Geological Society of America Digital Map and Chart Series 7. https://doi.org/10.1130/2010.dmch007.txt

Dyke, A.S., 2004. An outline of North American deglaciation with emphasis on central and northern Canada. Quat. Glaciat. Extent Chronol. 2, 373–424. https://doi.org/10.1016/s1571-0866(04)80209-4

Dyke, A.S., Moore, A., Robertson, L., 2003. Deglaciation of North America, Open File 1574. Geological Survey of Canada.

Fabel, D., Harbor, J., 1999. The use of in-situ produced cosmogenic radionuclides in glaciology and glacial geomorphology. Ann. Glaciol. 28, 103–110. https://doi.org/10.3189/172756499781821968

Fullerton, D.S., Colton, R.B., Bush, C.A., 2004. Limits of mountain and continental glaciations east of the Continental Divide in northern Montana and north-western North Dakota, U.S.A. Dev. Quat. Sci. 2, 131–150. https://doi.org/10.1016/s1571-0866(04)80194-5

Gosse, J.C., Klein, J., Lawn, B., Middleton, R., Evenson, E.B., 1995. Beryllium-10 Dating of the Duration and Retreat of the Last Pinedale Glacial Sequence. Science 268, 1329–1333. https://doi.org/10.1126/science.268.5215.1329

Guido, Z.S., Ward, D.J., Anderson, R.S., 2007. Pacing the post–Last Glacial Maximum demise of the Animas Valley glacier and the San Juan Mountain ice cap, Colorado. Geology 35, 739–742. https://doi.org/10.1130/g23596a.1

Harrison, S.P., Bartlein, P.J., Brewer, S., Prentice, I.C., Boyd, M., Hessler, I., Holmgren, K., Izumi, K., Willis, K., 2013. Climate model benchmarking with glacial and mid-Holocene climates. Clim. Dyn. 43, 671–688. https://doi.org/10.1007/s00382-013-1922-6

He, F., Shakun, J.D., Clark, P.U., Carlson, A.E., Liu, Z., Otto-Bliesner, B.L., Kutzbach, J.E., 2013. Northern Hemisphere forcing of Southern Hemisphere climate during the last deglaciation. Nature 494, 81–85. https://doi.org/10.1038/nature11822

Heyman, J., Applegate, P.J., Blomdin, R., Gribenski, N., Harbor, J.M., Stroeven, A.P., 2016. Boulder height – exposure age relationships from a global glacial 10Be compilation. Quat. Geochronol. 34, 1–11. https://doi.org/10.1016/j.quageo.2016.03.002

Hostetler, S., Clark, P.U., 1997. Climatic controls of Western U.S. Glaciers at the last glacial maximum. Quat. Sci. Rev. 16, 505–511. https://doi.org/10.1016/s0277-3791(96)00116-3

Hudson, A.M., Hatchett, B.J., Quade, J., Boyle, D.P., Bassett, S.D., Ali, G., Santos, M.G.D. los, 2019. North-south dipole in winter hydroclimate in the western United States during the last deglaciation. Sci. Rep. 9, 4826. https://doi.org/10.1038/s41598-019-41197-y

Huybers, K., Roe, G.H., 2009. Spatial Patterns of Glaciers in Response to Spatial Patterns in Regional Climate. J. Climate 22, 4606–4620. https://doi.org/10.1175/2009jcli2857.1

Hyndman, D.W., Thomas, R., 2020. Roadside Geology of Montana. Mountain Press Publishing.

Kohl, C.P., Nishiizumi, K., 1992. Chemical isolation of quartz for measurement of in-situ - produced cosmogenic nuclides. Geochim. Cosmochim. Acta 56, 3583–3587. https://doi.org/10.1016/0016-7037(92)90401-4

Laabs, B.J.C., Licciardi, J.M., Leonard, E.M., Munroe, J.S., Marchetti, D.W., 2020. Updated cosmogenic chronologies of Pleistocene mountain glaciation in the western United States and associated paleoclimate inferences. Quat. Sci. Rev. 242, 106427. https://doi.org/10.1016/j.quascirev.2020.106427

Laabs, B.J.C., Munroe, J.S., Best, L.C., Caffee, M.W., 2013. Timing of the last glaciation and subsequent deglaciation in the Ruby Mountains, Great Basin, USA. Earth Planet Sci. Lett. 361, 16–25. https://doi.org/10.1016/j.epsl.2012.11.018

Laabs, B.J.C., Refsnider, K.A., Munroe, J.S., Mickelson, D.M., Applegate, P.J., Singer, B.S., Caffee, M.W., 2009. Latest Pleistocene glacial chronology of the Uinta Mountains: support for moisture-driven asynchrony of the last deglaciation. Quat. Sci. Rev. 28, 1171–1187. https://doi.org/10.1016/j.quascirev.2008.12.012

Lal, D., 1988. In situ-produced cosmogenic isotopes in terrestrial rocks. Annu. Rev. Earth Planet Sci. 16, 355–388. https://doi.org/10.1146/annurev.ea.16.050188.002035

Leclercq, P.W., Oerlemans, J., 2012. Global and hemispheric temperature reconstruction from glacier length fluctuations. Clim. Dyn. 38, 1065–1079. https://doi.org/10.1007/s00382-011-1145-7

Leonard, E.M., Laabs, B.J.B., Schweinsberg, A.D., Russell, C.M., Briner, J.P., Young, N.E., 2017a. Deglaciation of the Colorado Rocky Mountains following the Last Glacial Maximum. Cuadernos De Investigación Geográfica 43, 497–526. https://doi.org/10.18172/cig.3234

Leonard, E.M., Laabs, B.J.C., Plummer, M.A., Kroner, R.K., Brugger, K.A., Spiess, V.M., Refsnider, K.A., Xia, Y., Caffee, M.W., 2017b. Late Pleistocene glaciation and deglaciation in the Crestone Peaks area, Colorado Sangre de Cristo Mountains, USA – chronology and paleoclimate. Quat. Sci. Rev. 158, 127–144. https://doi.org/10.1016/j.quascirev.2016.11.024

Licciardi, J.M., Clark, P.U., Brook, E.J., Elmore, D., Sharma, P., 2004. Variable responses of western U.S. glaciers during the last deglaciation. Geology 32, 81–84. https://doi.org/10.1130/g19868.1

Licciardi, J.M., Clark, P.U., Brook, E.J., Pierce, K.L., Kurz, M.D., Elmore, D., Sharma, P., 2001. Cosmogenic 3He and 10Be chronologies of the late Pinedale northern Yellowstone ice cap, Montana, USA. Geology 29, 1095–1098.

Licciardi, J.M., Pierce, K.L., 2018. History and dynamics of the Greater Yellowstone Glacial System during the last two glaciations. Quat. Sci. Rev. 200, 1–33. https://doi.org/10.1016/j.quascirev.2018.08.027

Licciardi, J.M., Pierce, K.L., 2008. Cosmogenic exposure-age chronologies of Pinedale and Bull Lake glaciations in greater Yellowstone and the Teton Range, USA. Quat. Sci. Rev. 27, 814–831. https://doi.org/10.1016/j.quascirev.2007.12.005

Lifton, N., Caffee, M., Finkel, R., Marrero, S., Nishiizumi, K., Phillips, F.M., Goehring, B., Gosse, J., Stone, J., Schaefer, J., Theriault, B., Jull, A.J.T., Fifield, K., 2015. In situ cosmogenic nuclide production rate calibration for the CRONUS-Earth project from Lake Bonneville, Utah, shoreline features. Quat. Geochronol. 26, 56–69. https://doi.org/10.1016/j.quageo.2014.11.002

Lifton, N., Sato, T., Dunai, T.J., 2014. Scaling in situ cosmogenic nuclide production rates using analytical approximations to atmospheric cosmic-ray fluxes. Earth Planet Sci. Lett. 386, 149–160. https://doi.org/10.1016/j.epsl.2013.10.052

Lisiecki, L.E., Raymo, M.E., 2005. A Pliocene-Pleistocene stack of 57 globally distributed benthic δ18O records. Paleoceanography 20. https://doi.org/10.1029/2004pa001071

Liu, Z., Otto-Bliesner, B.L., He, F., Brady, E.C., Tomas, R., Clark, P.U., Carlson, A.E., Lynch-Stieglitz, J., Curry, W., Brook, E.J., Erickson, D., Jacob, R., Kutzbach, J., Cheng, J., 2009. Transient Simulation of Last Deglaciation with a New Mechanism for Bolling-Allerod Warming. Science 325, 310–314. https://doi.org/10.1126/science.1171041

Locke, W., Smith, L.N., 2004. Pleistocene mountain glaciation in Montana, USA, in: Quaternary Glaciations-Extent and Chronology. Elsevier, pp. 125–129. https://doi.org/10.1016/s1571-0866(04)80193-3

Locke, W.W., 1990. Late Pleistocene glaciers and the climate of western Montana, USA. Arctic and Alpine Research 22, 1–13. https://doi.org/10.1080/00040851.1990.12002761

Lora, J.M., 2018. Components and Mechanisms of Hydrologic Cycle Changes over North America at the Last Glacial Maximum. J. Climate 31, 7035–7051. https://doi.org/10.1175/jcli-d-17-0544.1

Lora, J.M., Ibarra, D.E., 2019. The North American hydrologic cycle through the last deglaciation. Quat. Sci. Rev. 226, 105991. https://doi.org/10.1016/j.quascirev.2019.105991

Marchetti, D.W., Cerling, T.E., Dohrenwend, J.C., Gallin, W., 2007. Ages and significance of glacial and mass movement deposits on the west side of Boulder Mountain, Utah, USA.

Palaeogeogr. Palaeoclimatol. Palaeoecol. 252, 503–513. https://doi.org/10.1016/j.palaeo.2007.05.016

Marchetti, D.W., Cerling, T.E., Lips, E.W., 2005. A glacial chronology for the Fish Creek drainage of Boulder Mountain, Utah, USA. Quat. Res. 64, 264–271. https://doi.org/10.1016/j.yqres.2005.05.004

Marchetti, D.W., Harris, M.S., Bailey, C.M., Cerling, T.E., Bergman, S., 2011. Timing of glaciation and last glacial maximum paleoclimate estimates from the Fish Lake Plateau, Utah. Quat. Res. 75, 183–195. https://doi.org/10.1016/j.yqres.2010.09.009

Marcott, S.A., Clark, P.U., Shakun, J.D., Brook, E.J., Davis, P.T., Caffee, M.W., 2019. 10Be age constraints on latest Pleistocene and Holocene cirque glaciation across the western United States. NPJ Clim. Atmospheric Sci. 2, Article 5. https://doi.org/10.1038/s41612-019-0062-z

McDonald, C., Elliott, C.G., Vuke, S.M., Lonn, J.D., Berg, R.B., 2012. Geologic Map of the Butte South 30'X 60'Quadrangle, Southwestern, Montana. Montana Bureau of Mines and Geology.

McDonald, C., Yakovlev, P., 2019. Geologic Map of the Twin Adams Mountain 7.5' Quadrangle, Southwestern Montana. Montana Bureau of Mines and Geology.

Munroe, J.S., Laabs, B.J.C., Shakun, J.D., Singer, B.S., Mickelson, D.M., Refsnider, K.A., Caffee, M.W., 2006. Latest Pleistocene advance of alpine glaciers in the southwestern Uinta Mountains, Utah, USA: evidence for the influence of local moisture sources. Geology 34, 841–844. https://doi.org/10.1130/g22681.1

Munroe, J.S., Mickelson, D.M., 2002. Last Glacial Maximum equilibrium-line altitudes and paleoclimate, northern Uinta Mountains, Utah, U.S.A. J. Glaciol. 48, 257–266. https://doi.org/10.3189/172756502781831331

Nishiizumi, K., Imamura, M., Caffee, M.W., Southon, J.R., Finkel, R.C., McAninch, J., 2007. Absolute calibration of 10Be AMS standards. Nucl. Inst. and Meth. in Phys. Res. B 258, 403–413.

Nishiizumi, K., Kohl, C.P., Arnold, J.R., Dorn, R., Klein, I., Fink, D., Middleton, R., Lal, D., 1993. Role of in situ cosmogenic nuclides 10be and 26al in the study of diverse geomorphic processes. Earth Surf. Process. Landforms 18, 407–425. https://doi.org/10.1002/esp.3290180504

Oerlemans, J., 2005. Extracting a climate signal from 169 glacier records. Science 308, 675–677. https://doi.org/10.1126/science.1107046

Oster, J.L., Ibarra, D.E., Winnick, M.J., Maher, K., 2015. Steering of westerly storms over western North America at the Last Glacial Maximum. Nat. Geosci. 8, 201–205. https://doi.org/10.1038/ngeo2365

Pearson, R.C., Zen, E., 1985. Geologic map of the Eastern Pioneer Mountains, Beaverhead County, Montana (Report No. 1806A), Miscellaneous Field Studies Map.

Peel, M.C., Finlayson, B.L., McMahon, T.A., 2007. Updated world map of the Köppen-Geiger climate classification. Hydrol. Earth Syst. Sci. 11, 1633–1644.

Peltier, W., Fairbanks, R.G., 2006. Global glacial ice volume and Last Glacial Maximum duration from an extended Barbados sea level record. Quat. Sci. Rev. 25, 3322–3337.

Peltier, W.R., 2004. Global glacial isostasy and the surface of the ice-age Earth: the ICE-5G (VM2) model and GRACE. Annu. Rev. Earth Planet. Sci. 32, 111–149. https://doi.org/10.1146/annurev.earth.32.082503.144359

Phillips, F.M., Zreda, M., Plummer, M.A., Elmore, D., Clark, D.H., 2009. Glacial geology and chronology of Bishop Creek and vicinity, eastern Sierra Nevada, California. Geol. Soc. Am. Bull. 121, 1013–1033. https://doi.org/10.1130/b26271.1

Phillips, F.M., Zreda, M.G., Benson, L.V., Plummer, M.A., Elmore, D., Sharma, P., 1996. Chronology for Fluctuations in Late Pleistocene Sierra Nevada Glaciers and Lakes. Science 274, 749–751. https://doi.org/10.1126/science.274.5288.749

Phillips, F.M., Zreda, M.G., Gosse, J.C., 1997. Cosmogenic 36Cl and 10Be ages of Quaternary glacial and fluvial deposits of the Wind River Range, Wyoming. Geol. Soc. Am. Bull. 109, 1453–1463.

Phillips, F.M., Zreda, M.G., Smith, S.S., Elmore, D., Kubik, P.W., Sharma, P., 1990. Cosmogenic Chlorine-36 Chronology for Glacial Deposits at Bloody Canyon, Eastern Sierra Nevada. Science 248, 1529–1532. https://doi.org/10.1126/science.248.4962.1529

Pierce, K.L., 2003. Pleistocene glaciations of the Rocky Mountains. Dev. Quat. Sci. 1, 63–76. https://doi.org/10.1016/s1571-0866(03)01004-2

Pierce, K.L., Licciardi, J.M., Good, J.M., Jaworowski, C., 2018. Pleistocene glaciation of the Jackson Hole area, Wyoming (No. 1835). US Geological Survey. https://doi.org/10.3133/pp1835

Plummer, M.A., Phillips, F.M., 2003. A 2-D numerical model of snow/ice energy balance and ice flow for paleoclimatic interpretation of glacial geomorphic features. Quat. Sci. Rev. 22, 1389–1406. https://doi.org/10.1016/s0277-3791(03)00081-7

Porter, S.C., 1983. Late Wisconsin mountain glaciation in the western United States, in: Late-Quaternary Environments of the United States, Vol. 1. University of Minnesota, Minneapolis, pp. 71–111.

Porter, S.C., Swanson, T.W., 2008. 36Cl dating of the classic Pleistocene glacial record in the northeastern Cascade Range, Washington. Am. J. Sci. 308, 130–166. https://doi.org/10.2475/02.2008.02

Putnam, A.E., 2015. Palaeoclimate: A glacial zephyr. Nat. Geosci. 8, 175–176. https://doi.org/10.1038/ngeo2377

Quirk, B.J., Huss, E., Laabs, B.J.C., Leonard, E., Licciardi, J., Plummer, M.A., Caffee, M.W., 2022. Late Pleistocene glacial chronologies and paleoclimate in the northern Rocky Mountains. Clim. Past 18, 293–312. https://doi.org/10.5194/cp-18-293-2022

Quirk, B.J., Moore, J.R., Laabs, B.J.C., Caffee, M.W., Plummer, M.A., 2018. Termination II, Last Glacial Maximum, and Lateglacial chronologies and paleoclimate from Big Cottonwood Canyon, Wasatch Mountains, Utah. Geol. Soc. Am. Bull. 130, 1889–1902. https://doi.org/10.1130/b31967.1

Quirk, B.J., Moore, J.R., Laabs, B.J.C., Plummer, M.A., Caffee, M.W., 2020a. Latest Pleistocene glacial and climate history of the Wasatch Range, Utah. Quat. Geochronol. 238, 106313. https://doi.org/10.1016/j.quascirev.2020.106313

Quirk, B.J., Moore, J.R., Laabs, B.J.C., Plummer, M.A., Caffee, M.W., 2020b. Latest Pleistocene glacial and climate history of the Wasatch Range, Utah. Quaternary Sci Rev 238, 106313. https://doi.org/10.1016/j.quascirev.2020.106313

Refsnider, K.A., Laabs, B.J.C., Plummer, M.A., Mickelson, D.M., Singer, B.S., Caffee, M.W., 2008. Last glacial maximum climate inferences from cosmogenic dating and glacier modeling of the western Uinta ice field, Uinta Mountains, Utah. Quat. Res. 69, 130–144. https://doi.org/10.1016/j.yqres.2007.10.014

Roe, G.H., 2011. What do glaciers tell us about climate variability and climate change? J Glaciol 57, 567–578. https://doi.org/10.3189/002214311796905640

Roe, G.H., O'Neal, M.A., 2009. The response of glaciers to intrinsic climate variability: observations and models of late-Holocene variations in the Pacific Northwest. J. Glaciol. 55, 839–854. https://doi.org/10.3189/002214309790152438

Rood, D.H., Burbank, D.W., Finkel, R.C., 2011. Chronology of glaciations in the Sierra Nevada, California, from 10Be surface exposure dating. Quat. Sci. Rev. 30, 646–661. https://doi.org/10.1016/j.quascirev.2010.12.001

Ruppel, E.T., O'Neill, J.M., Lopez, D.A., 1993. Geologic map of the Dillon 1°x2° quadrangle, Idaho and Montana. U.S. Geological Survey.

Rupper, S., Roe, G., 2008. Glacier changes and regional climate: a mass and energy balance approach. J. Clim. 21, 5384–5401.

Schildgen, T.F., Phillips, W.M., Purves, R.S., 2005. Simulation of snow shielding corrections for cosmogenic nuclide surface exposure studies. Geomorphology 64, 67–85. https://doi.org/10.1016/j.geomorph.2004.05.003

Shakun, J.D., Clark, P.U., He, F., Marcott, S.A., Mix, A.C., Liu, Z., Otto-Bliesner, B., Schmittner, A., Bard, E., 2012. Global warming preceded by increasing carbon dioxide concentrations during the last deglaciation. Nature 484, 49–54. https://doi.org/10.1038/nature10915

Smith, L.N., 2007. Quaternary Geology of the Dillon Area, Beaverhead County, Montana, in: Northwest Geology. Northwest Geology, pp. 143–150.

Speth, G.T., Amos, C.B., Amidon, W.H., Balco, G., Meigs, A.J., Graf, S., 2018. Glacial chronology and slip rate on the west Klamath Lake fault zone, Oregon. Geol. Soc. Am. Bull. 131, 444–460. https://doi.org/10.1130/b31961.1

Stokes, C.R., Tarasov, L., Dyke, A.S., 2012. Dynamics of the North American Ice Sheet Complex during its inception and build-up to the Last Glacial Maximum. Quat. Sci. Rev. 50, 86–104. https://doi.org/10.1016/j.quascirev.2012.07.009

Thackray, G.D., 2008. Varied climatic and topographic influences on Late Pleistocene mountain glaciation in the western United States. J. Quat. Sci., Publ. Quat. Res. Assoc. 23, 671–681. https://doi.org/10.1002/jqs.1210

Thackray, G.D., Lundeen, K.A., Borgert, J.A., 2004. Latest Pleistocene alpine glacier advances in the Sawtooth Mountains, Idaho, USA: Reflections of midlatitude moisture transport at the close of the last glaciation. Geology 32, 225–228. https://doi.org/10.1130/g20174.1

Tulenko, J.P., Lofverstrom, M., Briner, J.P., 2020. Ice sheet influence on atmospheric circulation explains the patterns of Pleistocene alpine glacier records in North America. Earth Planet. Sci. Lett. 534, 116115. https://doi.org/10.1016/j.epsl.2020.116115

Ullman, D.J., Carlson, A.E., Hostetler, S.W., Clark, P.U., Cuzzone, J., Milne, G.A., Winsor, K., Caffee, M., 2016. Final Laurentide ice-sheet deglaciation and Holocene climate-sea level change. Quat. Sci. Rev. 152, 49–59. https://doi.org/10.1016/j.quascirev.2016.09.014

Ullman, D.J., LeGrande, A.N., Carlson, A.E., Anslow, F.S., Licciardi, J.M., 2014. Assessing the impact of Laurentide Ice Sheet topography on glacial climate. Clim. Past 10, 487–507. https://doi.org/10.5194/cp-10-487-2014-supplement

Wesnousky, S.G., Briggs, R.W., Caffee, M.W., Ryerson, F.J., Finkel, R.C., Owen, L.A., 2016. Terrestrial cosmogenic surface exposure dating of glacial and associated landforms in the Ruby Mountains-East Humboldt Range of central Nevada and along the northeastern flank of the Sierra Nevada. Geomorphology 268, 72–81. https://doi.org/10.1016/j.geomorph.2016.04.027

Wong, C.I., Potter, G.L., Montañez, I.P., Otto-Bliesner, B.L., Behling, P., Oster, J.L., 2016. Evolution of moisture transport to the western US during the last deglaciation. Geophys. Res. Lett. 3468–3477. https://doi.org/10.1002/2016gl068389

Ye, S., Cuzzone, J.K., Marcott, S.A., Licciardi, J.M., Ward, D.J., Heyman, J., Quinn, D.P., 2023. A quantitative assessment of snow shielding effects on surface exposure dating from a western North American 10Be data compilation. Quat. Geochronol. 76, 101440. https://doi.org/10.1016/j.quageo.2023.101440

Young, N.E., Briner, J.P., Leonard, E.M., Licciardi, J.M., Lee, K., 2011. Assessing climatic and nonclimatic forcing of Pinedale glaciation and deglaciation in the western United States. Geology 39, 171–174. https://doi.org/10.1130/g31527.1

Zimmerman, S.G., Evenson, E.B., Gosse, J.C., Erskine, C.P., 1994. Extensive Boulder Erosion Resulting from a Range Fire on the Type-Pinedale Moraines, Fremont Lake, Wyoming. Quat. Res. 42, 255–265. https://doi.org/10.1006/qres.1994.1076